



**Politecnico
di Torino**

M.Sc. Dissertation.
Master of Science in Petroleum Engineering
Department of Environment, Land and Infrastructure Engineering

**Optimizing Geothermal Energy Extraction
from Decommissioned Oil Wells:
The Case Study of the
Villafortuna-Treccate Oil Field**

Omid Binaei

Supervisors:

Prof. Glenda Taddia
Dr. Martina Gizzi

Politecnico di Torino
July, 2024

Abstract

Currently, there are 20-30 million decommissioned hydrocarbon wells worldwide, presenting an excellent opportunity for geothermal energy production. The debate over disused hydrocarbon wells revolves around whether to seal them to avoid potential issues or to reuse them to transition to sustainable energy. Shutting down these wells involves significant costs and challenges, including financial challenges, environmental risks such as pollution and methane leakage. One viable solution is to repurpose these wells to extract geothermal energy from existing deep hydrocarbon reservoirs, minimizing initial costs by 40 to 60% and resulting in revenue generation, reduction of leaking emissions, and maintenance of workforce involvement. Reusing of these wells must adapt to local energy demand, potential markets, existing infrastructure and technical obstacles. Until now, most studies have either been scattered or focused on determining if converting a particular wells is possible. The aim of this study is to assess the geothermal potential within the depleted Villafortuna-Trecate oil field in Italy. This will be achieved by utilizing information from the Ministry of Economic Development, published data on hydrocarbon fields, and estimated depth temperatures from the Italian National Geothermal Database. We will employ simplified closed-loop system models developed and applied to specific wells using Python to facilitate this assessment. The present study examines the feasibility of implementing a Coaxial Wellbore Heat eXchanger CWHX on four promising wells in one of the Europe's largest and deepest oilfields, the Villafortuna-Trecate oilfield, with a focus on optimizing the WHX for maximum heat extraction. The study concludes that while challenges exist, such as high initial costs and technical complexities, repurposing these wells can generate sustainable energy and reduce environmental impact, particularly through district heating applications and industrial processes.

Acknowledgments

I would like to express my sincere gratitude to:

Professor Martina Gizzi for her invaluable support, guidance, and patience.

Professor Glenda Taddia for her professional guidance and expertise.

Dr. Sam Abbasi, the best roomie, for his support and guidance.

My friends for their presence and the enjoyable moments we've shared.

Torino for being the most lovely city in the world, my second home forever.

Dedication

This thesis is dedicated to my family:

To my mother, the first and the last “love”.

To my father, who truly defines the word “man”.

To my sister, the most lovely and sweet presence in my life.

For their endless love, support, and encouragement.

Contents

1.	Introduction.....	1
1.1.	Renewable Energy	1
1.2.	Geothermal Energy	1
2.	Literature Review	3
2.1.	Introduction.....	3
2.2.	Potential of Using Geothermal Resources in Italy.....	3
2.3.	Italian Petroleum Systems	4
2.4.	Thermophysical Features of the Po Basin Rocks	6
2.5.	Villafortuna-Trecate Oil Field.....	9
2.6.	Geothermal Technologies for Well Repurposing.....	10
2.7.	Coaxial Wellbore Heat eXchanger.....	11
3.	Methodology	12
3.1.	Introduction.....	12
3.2.	Data Collection	12
3.3.	Determining Thermal Properties	13
3.4.	Coaxial Wellbore Heat eXchanger Model	16
3.4.1.	Rock Temperature Evaluation.....	17
3.4.2.	Transfer of Heat Within the Pipe System.....	17
3.4.3.	Heat Transfer Rate and Electrical Power Evaluation	21
3.4.4.	Pressure Losses and Pumping Power Consumption Evaluation	22
3.4.5.	Assumptions and Estimations	23
4.	Results and Discussion	25
4.1.	Long-Term CWHX System Performance.....	26
4.1.1.	Comparison of 2-Year and 10-Year Performance	27

4.2.	Flow Rate Impact on System Performance.....	28
4.2.1.	Flow Rate Impact on Pressure Losses.....	30
4.2.2.	Flow Rate Impact on Temperature and Thermal Efficiency	31
4.2.3.	Flow Rate Impact on Pumping Power (Wcp)	32
4.3.	Configuration Impact on System Performance.....	33
4.4.	The Impact of Flow Rate and Configuration on Thermal and Electrical Power Generation	39
4.4.1.	Thermal Power Generation	39
4.4.2.	Electrical Power Generation	39
4.5.	Possible Application of Case Studies	40
4.5.1.	Potential Applications for Generated Electrical Power.....	40
4.5.2.	Potential Applications for Generated Thermal Power.....	41
4.6.	Limitations and Challenges	41
5.	Conclusion	43
5.1.	Key Findings.....	43
5.2.	Future Work	44
	References:	46

List of Figures

Figure 1-1 Lindal diagram illustrating applications of geothermal fluids based on temperature. ORC represents the Organic Rankine Cycle [5].	2
Figure 2-1 The geographic location of the five petroleum systems recognised in Italy (right), stratigraphic distribution of the related source rocks and hydrocarbon occurrences (left) [10].	5
Figure 2-2 Petroleum exploration stratigraphy in the western Po Plain [8].	5
Figure 2-3 Location of wells (full circles) whose core specimens were used for laboratory measurements	7
Figure 2-4 Vertical thermal conductivity <i>kin</i> of the Mortara and Turbigo wells as inferred from lithostratigraphic information. Formation names are indicated.	8
Figure 2-5 Wells and Municipalities in Villafortuna-Trecate Field.	9
Figure 2-6 Production data of the Villafortuna-Trecate oil field, highlighting its decline and end of life (current production ceased) [15].	10
Figure 2-7 Geothermal closed-loop systems, A (U-tube) and B (Coaxial double-pipe) technologies	11
Figure 2-8 Coaxial Wellbore heat exchanger (CWHX). Cross section and schematic.	11
Figure 3-1 Temperature data (°C) vs depth (m) visualization.	13
Figure 3-2 CWHX geometry: considered configuration [21].	16
Figure 3-3 Thermal influence radius	19
Figure 3-4 Flowchart modeling implemented using Python	23
Figure 4-1 Performance Analysis after 2 Years for 2.7 kg/s Flow Rate with Alimonti Configuration	26
Figure 4-2 Performance Analysis after 10 Years for 2.7 kg/s Flow Rate with Alimonti Configuration	26
Figure 4-3 Performance analysis for Galliate 1 with the Alimonti configuration at different flow rates	29
Figure 4-4 Performance analysis for Trecate 10 with the Alimonti configuration at different flow rates	29

Figure 4-5 Performance analysis for Villafortuna 4 with the Alimonti configuration at different flow rates	30
Figure 4-6 Performance analysis for Turbigo 1 with the Alimonti configuration at different flow rates	30
Figure 4-7 Impact of Flow Rate on Wellhead Temperature	31
Figure 4-8 Impact of Flow Rate on Heat Transfer Rate (Thermal Power)	32
Figure 4-9 Impact of Flow Rate on Pumping Power Required (Wcp)	33
Figure 4-10 Performance Analysis for Turbigo1 at 2.7 kg/s Flow Rate & Different Configurations	34
Figure 4-11 Performance Analysis for Trecate10 at 2.7 kg/s Flow Rate & Different Configurations	34
Figure 4-12 Performance Analysis for Galliate1 at 2.7 kg/s Flow Rate & Different Configurations	35
Figure 4-13 Performance Analysis for Villafortuna4 at 2.7 kg/s Flow Rate & Different Configurations	35

List of Tables

Table 2-1. Laboratory results of physical properties. k_r is the thermal conductivity of water-saturated isotropic (code 1–5 and 9–18) samples, ϕ is the porosity, ρ_{rcr} and ρ_r are the volumetric heat capacity and the density, respectively, of both isotropic and anisotropic (code 6–8) dry samples. The standard deviation (in brackets) and the number n of samples are listed.....	7
Table 3-1 Ternal gradient	13
Table 3-2 GALLIATE 1	14
Table 3-3 Trecate 10.....	14
Table 3-4 Villafortuna 4	15
Table 3-5 Turbigio 1	15
Table 3-6 Geometry of BHE	16
Table 3-7 Constant Fluid Properties.....	24
Table 4-1 Performance Metrics for 2.7 kg/s Flow Rate with Alimonti Configuration after 2 Years	27
Table 4-2 Performance Metrics for 2.7 kg/s Flow Rate with Alimonti Configuration after 10 Years	27
Table 4-3 Simulation Results for Different Wells, Flow Rates, and Geometry Configurations.....	37
Table 4-4 Simulation Results for Different Wells, Flow Rates, and Geometry Configurations.....	38
Table 4-5 Summation of Thermal Power Outputs for Different Flow Rates & Configurations of all 4 wells	39
Table 4-6 Total Daily Electrical Power Generated for Different Flow Rates & Configurations of all wells	39

Nomenclature

Parameter	Symbol	Unit of Measure
Specific heat capacity of the water	$c_{p,w}$	[Jkg ⁻³ K ⁻¹]
Specific heat capacity of the rock	$c_{p,s}$	[Jkg ⁻³ K ⁻¹]
Density of rock	ρ_s	[kgm ⁻³]
Density of fluid	ρ_f	[Wm ⁻¹ K ⁻¹]
Thermal conductivity of the rock	λ_s	[Wm ⁻¹ K ⁻¹]
Hydraulic diameter	D_h	[mm]
Thermal conductivity of the pipe material	λ_j	[Wm ⁻¹ K ⁻¹]
Viscosity	μ	[mm Pa s]
Rock's thermal diffusivity	α_s	[ms ⁻¹]
Radius of thermal influence	r_s	[m]
Temperature of fluid	T_f	[°C]
Local geothermal gradient	GT	[°C]
Rock temperature at depth z	$T_s(z)$	[°C]
Mean ground surface temperature	T_g	[°C]
Pressure losses	ΔP	[k Pa]
Electrical power generated from the thermal energy	W_e	[MWh]
Electrical power required to circulate fluids	W_{cp}	[kW]
Flow rate	\dot{m}	[kgs ⁻¹]
Fluid velocity	v_f	[ms ⁻¹]
Thermal power	Q	[kW]
Heat flux	\dot{Q}	[W]
Heat exchange coefficient	\bar{U}	[m ⁻² K ⁻¹]
Convective heat transfer coefficient to the exterior wall	h_o	[Wm ⁻² K ⁻¹]
Time	t'	[h]
Composite pipe thickness	d	[mm]
Inner pipe radius	r_i	[mm]
Material radius	r_j	[mm]
Radius of the external casing	r_c	[mm]
Well's external radius	r_w	[mm]
Variation in length of the pipe	ΔL	[m]

Chapter 1

1. Introduction

1.1. Renewable Energy

Transitioning to renewable energy is essential for addressing climate change, the energy crisis, and securing a sustainable future. Renewable sources offer environmentally friendly and inexhaustible energy, contrasting with fossil fuels that contribute to climate change, air pollution, and health problems [1]. Fossil fuels are finite and jeopardize energy security and economic stability. Embracing renewables not only mitigates climate impacts and improves air quality but also enhances energy security for future generations [2].

1.2. Geothermal Energy

Geothermal energy, originating from the Earth's core through heat generated during planetary formation and radioactive decay, stands out due to its vast potential as a sustainable resource available in nearly every corner of the earth [3]. Despite its widespread availability, geothermal energy is often overlooked and underestimated due to challenges in extraction, insufficient research, and inadequate investment.

Renewable and environmentally friendly energy sources, such as geothermal energy, are fundamental to modern global energy systems. Unlike other renewables susceptible to weather fluctuations, geothermal energy provides reliable, consistent power generation. This reliability aligns with sustainable development principles and environmental preservation.

Geothermal energy presents diverse opportunities depending on geological and hydrogeological factors like temperature, flow rate, and geothermal gradient. These opportunities include electricity generation, industrial processes, heating, energy storage, agriculture, and low-temperature applications through heat pumps. While high geothermal gradients are rare but ideal for direct energy extraction, geothermal energy is adaptable across various environments for different uses. It is categorized into high enthalpy ($>150^{\circ}\text{C}$) suitable for power generation and low enthalpy ($<100^{\circ}\text{C}$) for direct heating applications [4]. The Lindal diagram in Figure 1-1 showcases the diverse range of potential applications and their associated temperature requirements [5].

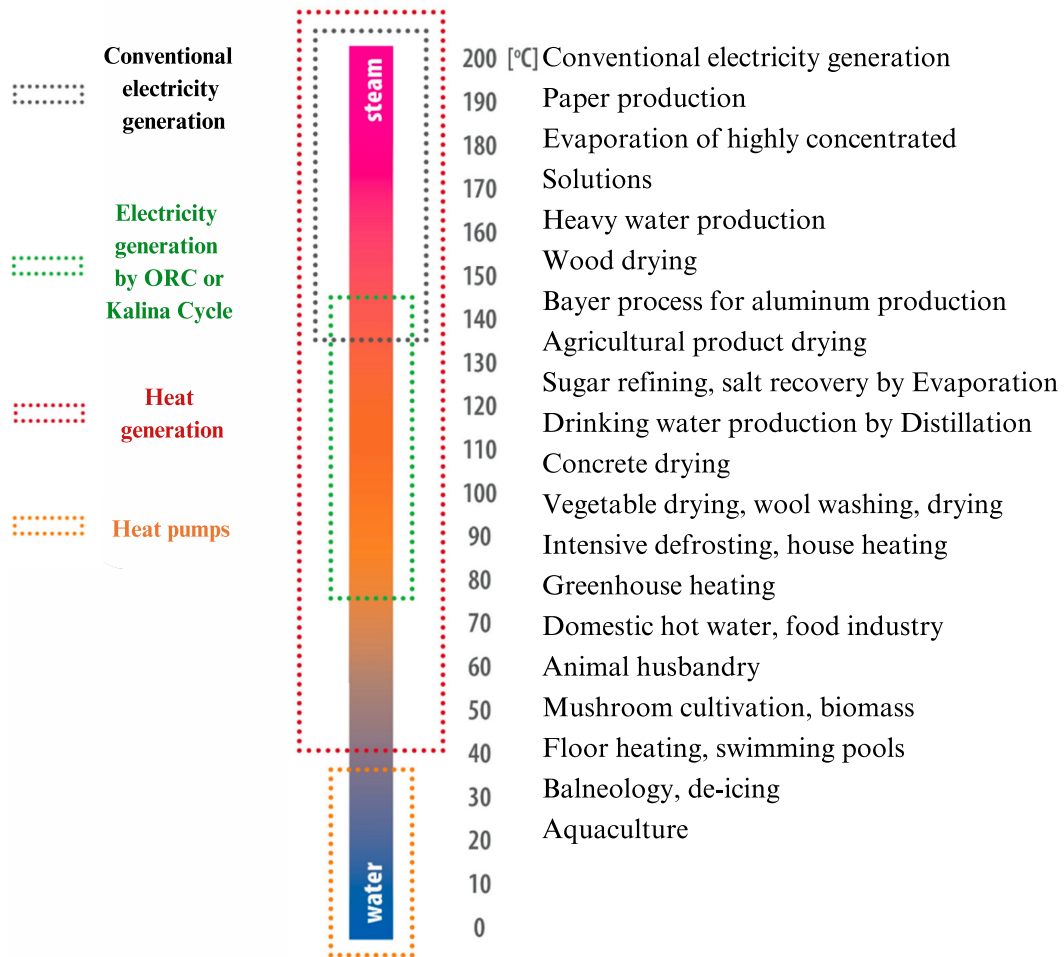


Figure 1-1 Lindal diagram illustrating applications of geothermal fluids based on temperature. ORC represents the Organic Rankine Cycle [6].

Chapter 2

2. Literature Review

2.1. Introduction

The aim of this literature review is to thoroughly examine existing research on the adaptation of abandoned hydrocarbon wells for geothermal energy production. The review specifically focuses on methodologies for converting these wells into effective geothermal systems, and investigates the geological and thermophysical properties of rock types within Italy's Po Plain, particularly around the Villafortuna-Trecate oil field. By integrating insights from prior studies, this review aims to establish a well-informed basis for the practical application and evaluation of such conversions in this thesis.

2.2. Potential of Using Geothermal Resources in Italy

Geothermal energy exploitation in Italy, which traces back to the early 1900s, began significantly in Tuscany. The Etruscans historically utilized geothermal heat, and the world's first geothermal power plant was inaugurated in Larderello, Pisa. This plant marked the start of over a century of geothermal innovation, transitioning from using natural steam as a coal alternative to modern operations involving deep well drilling over 4 km to harness geothermal fluids for electricity via steam turbines [7].

Italy is one of Europe's top geothermal energy producers, with an installed capacity of 1,100 MW at the Larderello plant alone, which contributes 6 TWh annually or 5% of the nation's green energy. Despite its pioneering status, the overall growth in geothermal capacity has been modest, with just a 10% increase from 2007 to 2017. As of the EGEN Geothermal Market Report 2020, Italy leads in installed capacity with 1,086 MW, significantly outpacing other central and northern European nations.

Italy holds immense geothermal potential estimated between 500 million and 10 billion tons of oil equivalent, translating to 5,800 to 116,000 TWh of energy. This far exceeds the annual national energy requirement of just over 300 TWh, suggesting that tapping even a small fraction of this resource could satisfy all domestic energy needs. Moving forward, the 2020s will focus on exploiting resources with temperatures of at least 90°C. By the 2030s, new technologies are expected to facilitate the use of lower-temperature, non-conventional geothermal sources. Projected expansions estimate the installed capacity for geothermoelectric energy could rise to between 1,070 and 1,140 MW by 2030, with a potential increase to between 2,000 and 2,500 MW by 2050. Correspondingly, annual production may grow to reach 7 TWh by 2030 and between 13 to 16 TWh by 2050, enabling geothermal energy to contribute 3-5% to Italy's energy needs, potentially expanding beyond Tuscany to account for 5-6% of national production by 2030 and 30-40% by 2050 [8].

2.3. Italian Petroleum Systems

This section provides an analysis of the primary geological configurations of major petroleum systems in Italy and their active hydrocarbon fields to set the context for our detailed case study evaluations.

In Italy, hydrocarbon indications (including fields, discoveries, and shows) are found in both carbonate and siliciclastic reservoir rocks. These rocks span a wide age range from the Triassic to the Paleogene and from the Oligocene to the Pleistocene. These reservoirs are situated across diverse geological environments such as thrust belts, foredeep basins, and foreland areas as depicted in Figure 2-1.

Research identifies at least five significant petroleum systems in Italy [9], based on key source rocks detailed in [9,10] and additional literature. The geographic scope and stratigraphic range of these systems, along with associated source rocks and hydrocarbon signs, are illustrated in Figure 2-1.

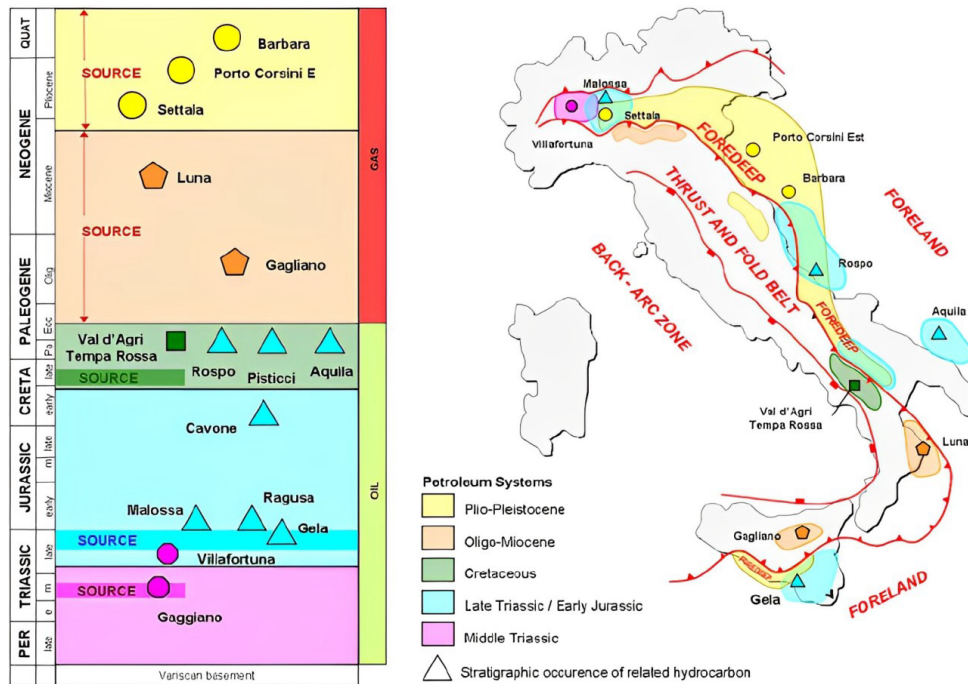


Figure 2-1 The geographic location of the five petroleum systems recognised in Italy (right), stratigraphic distribution of the related source rocks and hydrocarbon occurrences (left) [11].

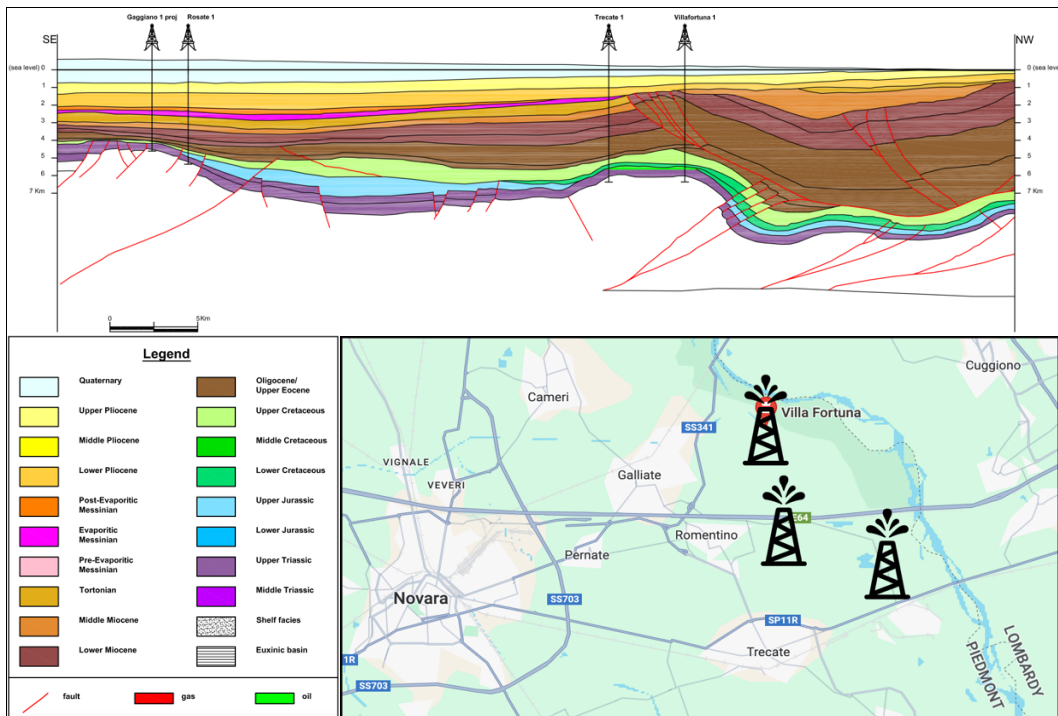


Figure 2-2 Petroleum exploration stratigraphy in the western Po Plain [9].

Three systems, predominantly oil-prone, formed from Meso-Cenozoic passive margin sedimentary covers. These covers consist of shallow water and pelagic carbonates, evaporites, and clastics deposited after Mesozoic extensional tectonics. One major system among these three is the Villafortuna-Trecate field, located in the western Po Plain (Figure 2-2). The remaining two systems are predominantly gas-prone, originating from terrigenous Oligo-Miocene and Plio-Pleistocene foredeep units created during the development of the Apennines and Alpine orogens [12].

In this research, we concentrate on evaluating the geothermal resources associated with abandoned wells located within the Villafortuna–Trecate oil field.

2.4. Thermophysical Features of the Po Basin Rocks

The Po Basin Figure 2-3, a vast sedimentary basin enclosed by the Alps and Apennines in Italy, has been thoroughly analyzed for its geothermal properties with a focus predominantly on heat conduction as the primary heat transfer mechanism.

In their study, Pasquale et al. (2011) analyzed thermal data from various wells to identify potential convective effects influencing the regional aquifer's thermal regime [13]. To supplement their analysis, laboratory measurements were conducted on rock samples extracted from multiple petroleum wells across the basin to assess their thermal properties, density, and porosity. These results supported mixing models to predict thermal conductivity and volumetric heat capacity precisely.

Detailed examination of over 100 core samples from depths up to 6,500 *m* revealed a diverse range of sedimentary, biochemical, and minor volcanic lithologies. The results are summarized in Table 2-1, which lists the investigated rocks by their origin, composition, and the number of available samples for each lithotype. Figure 2-4 illustrates The lithostratigraphic column and in situ thermal conductivity for the Mortara and Turbigio wells, where thermal conductivity generally increases with depth, primarily affected by compaction over temperature effects in initial layers. The highest conductivity values are observed in the deepest formations such as dacites and dolomites, while horizons of shales, silty shales, and siltstones at various depths show minimum values, indicating the impact of thermally anisotropic sheet silicates which can lead to constant or decreasing conductivity with depth.



Figure 2-3 Location of wells (full circles) whose core specimens were used for laboratory measurements

Table 2-1. Laboratory results of physical properties. k_r is the thermal conductivity of water-saturated isotropic (code 1–5 and 9–18) samples, ϕ is the porosity, $\rho_r c_r$ and ρ_r are the volumetric heat capacity and the density, respectively, of both isotropic and anisotropic (code 6–8) dry samples. The standard deviation (in brackets) and the number n of samples are listed.

Rock	Code/Lithotype	n	k_r ($W\ m^{-1}\ K^{-1}$)		$\rho_r c_r$ ($kJ\ m^{-3}\ K^{-1}$)		ϕ (per cent)		ρ_r ($kg\ m^3$)	
			Range	Mean	Range	Mean	Range	Mean	Range	Mean
Clastic	1- Marl	19	2.15-3.08	2.77 (0.23)	1310-2038	1808 (176)	6.0-37.0	15.1 (8.4)	1787-2530	2278 (240)
	2- Silty marl	18	2.85-3.66	3.16 (0.26)	1790-2150	1937 (125)	2.0-20.0	12.8 (5.5)	2150-2670	2359 (156)
	3- Calcareous marl	6	1.99-2.37	2.17 (0.13)	1406-1617	1495 (72)	22.0-35.0	30.8 (5.0)	1693-2008	1801 (123)
	4- Argillaceous limestone	3	3.58-3.63	3.60 (0.03)	1977-2094	2036 (59)	7.5-12.0	9.3 (2.4)	2477-2588	2520 (80)
	5- Argillaceous sandstone	6	2.60-3.40	3.00 (0.29)	1630-2059	1884 (155)	8.0-25.0	15.1 (6.2)	1990-2560	2330 (222)
	6- Siltstone	4	—	—	1853-2145	2003 (119)	6.0-18.0	11.1 (5.4)	2368-2560	2492 (107)
	7- Shale	6	—	—	1780-1970	1854 (63)	4.8-22.0	15.9 (6.3)	2120-2400	2220 (106)
	8- Silty shale	6	—	—	1680-1830	1739 (55)	5.0-21.0	13.2 (6.3)	2200-2570	2340 (145)
	9- Calcareneite	3	2.18-2.50	2.34 (0.16)	1370-1810	1590 (220)	25.0-32.0	29.0 (3.6)	1834-1997	1917 (82)
Chemical bio- chemical	Carbonate 10- Mudstone	5	3.04-3.48	3.30 (0.16)	2090-2188	2148 (36)	0.5-6.0	2.7 (2.1)	2550-2695	2630 (59)
	11- Wackestone	5	3.10-3.20	3.16 (0.04)	1980-2190	2108 (80)	3.0-10.0	6.0 (3.0)	2500-2670	2590 (75)
	12- Packstone	4	3.00-3.45	3.23 (0.18)	2014-2109	2058 (39)	3.0-6.0	4.3 (1.3)	2550-2655	2620 (59)
	13- Grainstone	5	2.95-3.36	3.12 (0.16)	1950-2070	2010 (55)	6.5-12.0	8.8 (2.5)	2400-2540	2480 (73)
	14- Dolostone	5	4.25-5.45	4.60 (0.49)	2240-2400	2331 (58)	1.5-7.5	3.8 (2.4)	2800-2630	2735 (73)
	Siliceous 15- Radiolarite	4	3.16-3.46	3.37 (0.14)	1953-2107	2021 (69)	0.5-5.5	2.4 (2.2)	2550-2650	2600 (48)
	Evaporitic 16- Anhydrite	5	3.15-3.65	3.39 (0.22)	1930-1970	1945 (17)	0.5-5.0	2.7 (1.8)	2680-2780	2730 (52)
17- Gypsum	5	1.40-1.64	1.54 (0.09)	2325-2500	2445 (71)	0.5-7.0	2.4 (2.6)	2260-2400	2350 (61)	
Igneous	Effusive 18- Dacite	4	3.56-3.91	3.73 (0.18)	2140-2160	2151 (8)	1.5-7.5	3.3 (2.8)	2690-2500	2610 (102)

As practical examples of this comprehensive assessment, the Mortara well, reaching a depth of 5,905 m, is situated above a structural high of a Tertiary volcanic edifice buried beneath the Miocene-Quaternary clastic cover. The Turbigo well extends even deeper to 6,631 m, tapping into a Mesozoic structural high (Figure 2-4). The well-documented lithostratigraphic sequences of both wells provide detailed insights into the subsurface thermal characteristics critical for evaluating the geothermal potential of the Po Basin [13].

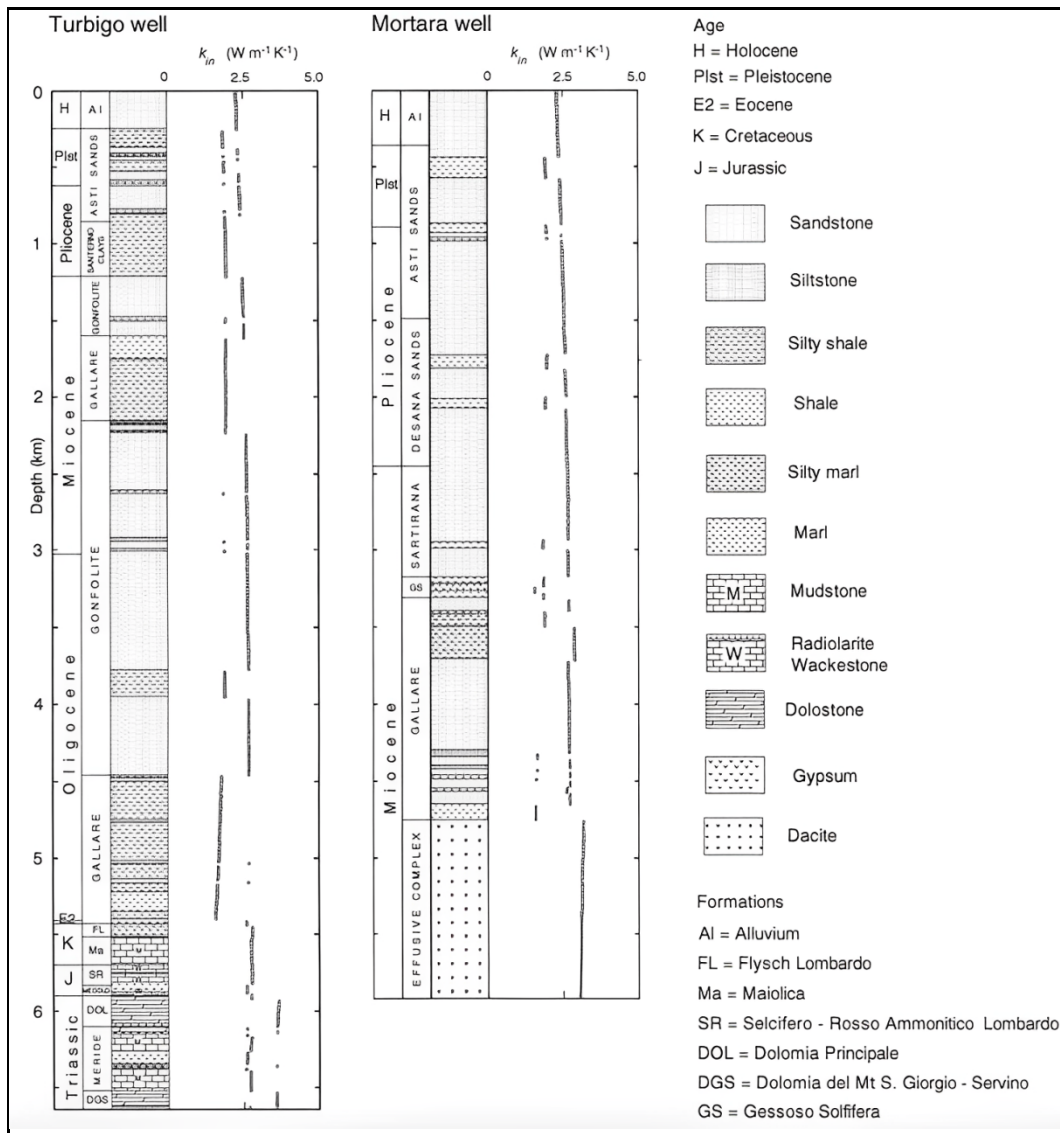


Figure 2-4 Vertical thermal conductivity k_{in} of the Mortara and Turbigo wells as inferred from lithostratigraphic information. Formation names are indicated.

2.5. Villafortuna-Trecale Oil Field

The Villafortuna–Trecale reservoir, recognized as one of the major oilfields in Europe, is positioned in the Piemonte region of northern Italy, adjacent to the municipalities of Novara, Trecale, Romentino, and Galliate, (Figure 2-5).

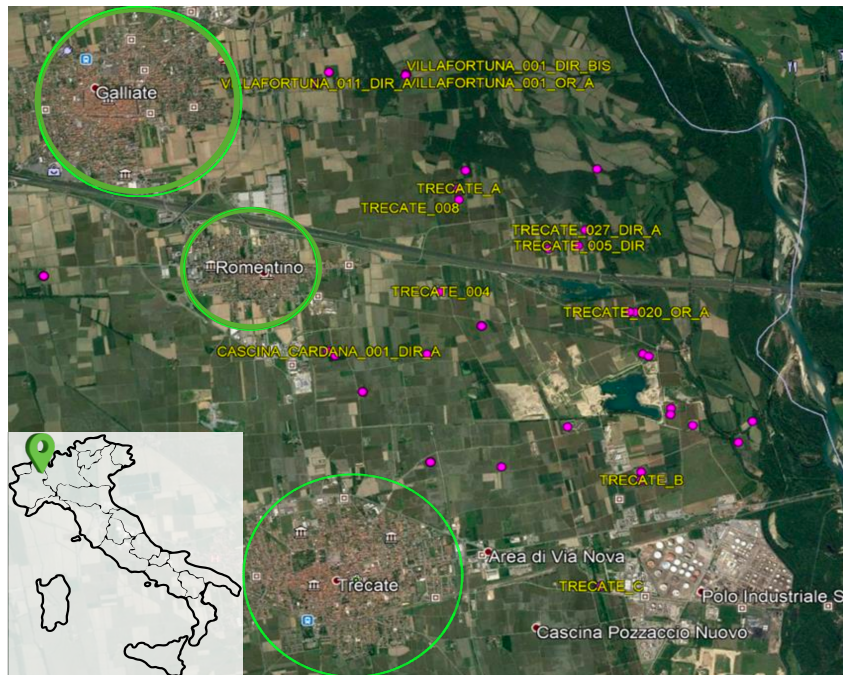


Figure 2-5 Wells and Municipalities in Villafortuna-Trecale Field.

The field features a main reservoir located at depths of 5700 to 6100 *m*, which makes it one of the deepest hydrocarbon deposits. Characterized by a temperature of approximately 166°C and an average static pressure of 850 bar, it represents a significant example of deep geothermal potential [14].

Whenever the Villafortuna-Trecale field had been discovered in the western Po Valley in 1984, it was predicted to contain 300 *MMbbl* of oil in place [15]. Production officially commenced in 1989, with an initial flow rate of roughly 13,000 *m*³/*d*. Field production data indicates that, as of the end of 2013, 3.6×10^4 *m*³ of oil and 2.7×10^9 *m*³ of gas had been produced.

Currently, the development of the Villafortuna-Trecale oil field has reached the end of its productive life. Data sourced from the Ministry of Economic Development (MSE, 2014), illustrated in Figure 2-6, confirms both this production tail and the approaching end of field life [14].

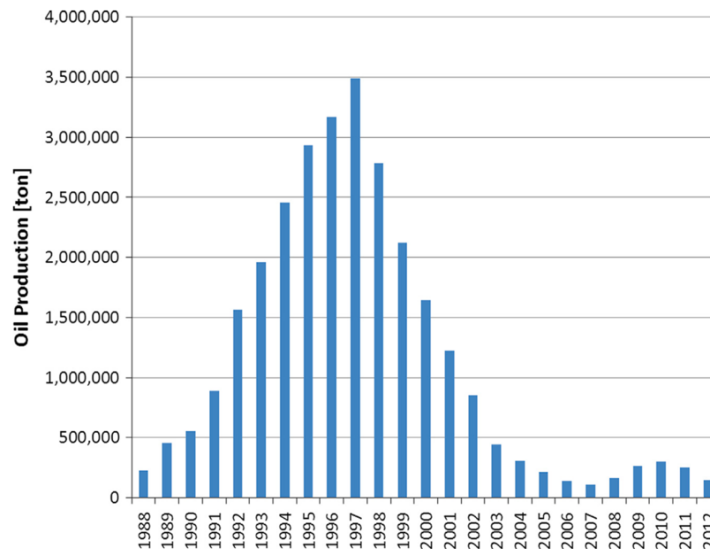


Figure 2-6 Production data of the Villafortuna-Trecate oil field, highlighting its decline and end of life (current production ceased) [16].

2.6. Geothermal Technologies for Well Repurposing

Repurposing decommissioned hydrocarbon wells for geothermal energy extraction involves retrofitting the borehole with a heat exchanger, leveraging abandoned oilfield infrastructure to tap into geothermal resources sustainably. Two primary geothermal closed-loop systems, U-tube and Coaxial double-pipe technologies (Figure 2-7), are commonly utilized for this purpose, this innovative approach extracts heat using a closed-loop heat carrier fluid circulation, eliminating geothermal fluids production and reducing environmental impact and energy requirements for reinjection [17]. In U-tube heat exchangers, fluid circulates through a single tube string, absorbing heat from surrounding geological formations, whereas coaxial heat exchangers employ two concentric pipes for fluid circulation. By avoiding corrosion and scaling issues, WHX presents a viable solution, albeit with potential reductions in heat recovery efficiency. The feasibility of WHX power plants hinges on factors such as flow rates, thermal insulation, local geothermal gradients, well depth, and heat carrier fluid properties [18]. Numerical models have explored the feasibility of WHX in existing geothermal wells and repurposed oil wells, highlighting the economic advantages of utilizing oil wells for WHX implementation. This approach significantly reduces abandonment costs and enhances the economic viability of geothermal plants by eliminating drilling expenses, which usually represent a significant portion of project costs. In this context, we'll delve into the coaxial method in detail [11].

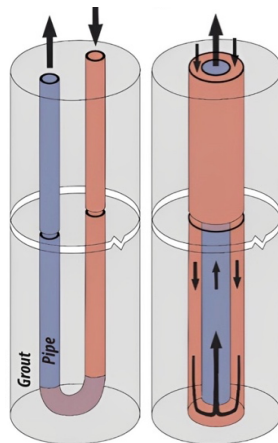


Figure 2-7 Geothermal closed-loop systems, A (U-tube) and B (Coaxial double-pipe) technologies

2.7. Coaxial Wellbore Heat eXchanger

The coaxial wellbore heat exchanger (CWHX) is a closed-loop geothermal system installed by inserting one pipe within another in a wellbore (Figure 2-8). The outer pipe acts as the injection pipe, conveying the working fluid downward to capture heat from rocks, while the inner pipe functions as the extraction pipe, carrying the warmed fluid back up. An insulating material typically fills the gap between the tubes to minimize heat loss during the upward flow. The CWHX offers a larger heat exchange surface area than U-tube systems, potentially leading to improved heat extraction efficiency. Additionally, grouting the space between the outer tube and the wellbore prevents fluid leakage and enhances heat transfer from the surrounding rock [18].

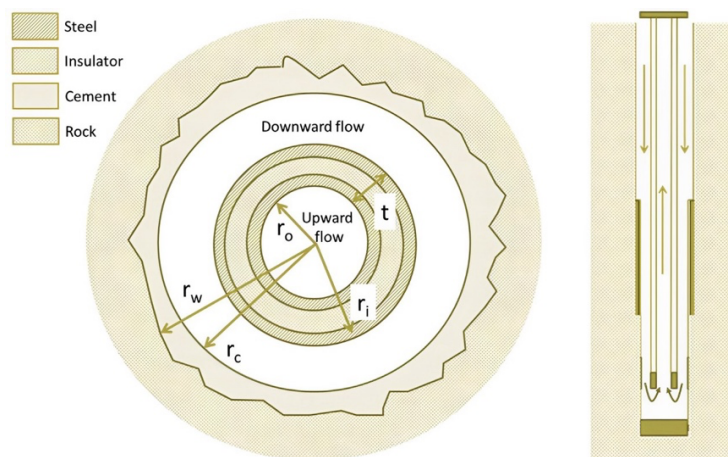


Figure 2-8 Coaxial Wellbore Heat eXchanger (CWHX). Cross section and schematic.

Chapter 3

3. Methodology

3.1. Introduction

This chapter describes the methods currently employed to investigate the potential of retrofitting decommissioned hydrocarbon wells within the Villafortuna-Trecate oilfield to harness geothermal energy resources using Coaxial Wellbore Heat eXchange system (CWHX). This methodology is chosen to assess well reuse feasibility, potential energy production, and associated limitations. This chapter outlines the data sources, calculates critical thermal properties, and describes the design of the computational model used for analysis.

3.2. Data Collection

Source: Data pertaining to the Villafortuna-Trecate oilfield was obtained from the National Geothermal Data Bank (BDNG) accessible through the GeoThopica portal of the Institute of Geosciences and Earth Resources of the National Research Council (CNR-IGG)[19].

Well Selection: Four wells were selected for analysis based on their depth, availability of detailed data, and abandonment status. Selection criteria considered factors impacting geothermal potential and well integrity. The following data types were collected for each well:

- **Well Name and Location:** Identification and geographical details.
- **Depth and Stratigraphy:** Detailed logs of well depth, including top and bottom depths of geological formations.
- **Formation Details:** Composition, age, and rock layer lithostratigraphy.
- **Temperature Data:** Gradient and specific temperature measurements at various depths, as reported in Table 3-1 and Figure 3-1.
- **Well Status:** Information on whether the wells, productive or abandoned.

These data points are critical for evaluating the feasibility and potential effectiveness of converting abandoned oil wells into geothermal energy sources.

Table 3-1 Thermal gradient

Well Name	Depth (m)	Thermal Gradient (°C/km)
Galliate 1	6694	26
Trecate 10	6560	26
Villafortuna 4	6550	30
Turbigo 1	6630	26

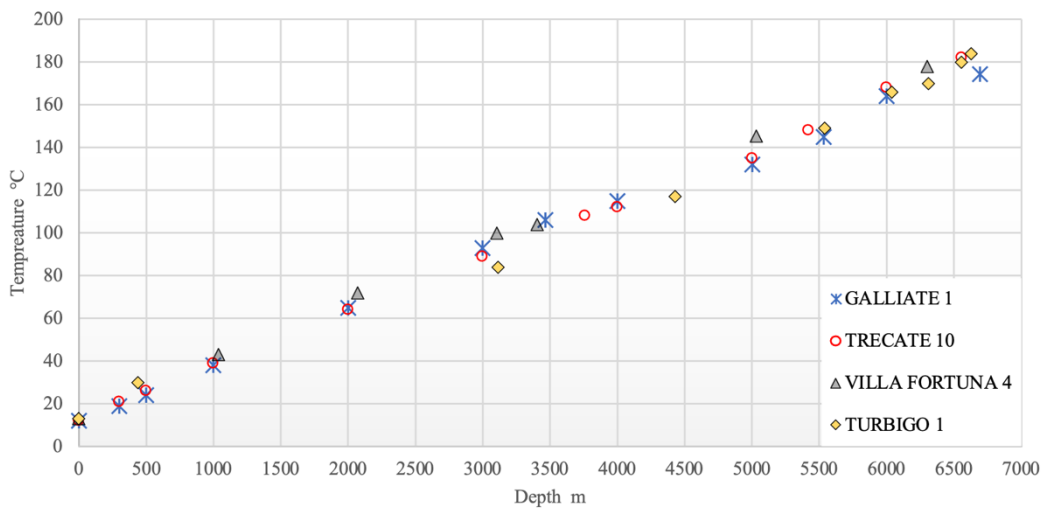


Figure 3-1 Temperature data (°C) vs depth (m) visualization.

3.3. Determining Thermal Properties

Since the specific lithological configurations at the studied wells differed from those described in existing literature, it was essential to calculate thermal conductivity, density, and specific heat capacity for each depth interval. To achieve this:

Literature Review: A comprehensive literature review was performed, including "Determination of Thermal Conductivity of Coarse and Fine Sand Soils" (Handman & Clark, 2010) and "Thermophysical Properties of the Po Basin Rocks" (Pasquale et al., 2011). This literature informed the selection of appropriate values and equations for the observed lithologies [20,21].

Calculations: Calculations were undertaken to determine the thermal conductivity λ_s , density ρ , and specific heat capacity $c_{p,s}$, of each geological layer. The specific methodologies applied were dependent on the lithology and were aligned with established approaches detailed in the reviewed literature.

Table 3-2 GALLIATE 1

Top	Bottom	Lithology	Thickness (m)	Age	λ_s (W/mK)	$c_{p,s}$ (J/kg·K)	ρ (kg/m ³)
0	1380	Alluvium,Sand,Clay	1380	Pleistocene	2,90	1471	2090
1380	5488	Sandstone, Conglomerate, Marl	4108	Miocene	2,95	1359	2427
5488	5690	Limestone	202	Lower Eocene	2,6	921	2600
5690	6645	Marl, Limestone and Dolomite	955	Albian	3,3	899	2538

Table 3-3 Trecate 10

Top	Bottom	Lithology	Thickness (m)	Age	λ_s (W/mK)	$c_{p,s}$ (J/kg·K)	ρ kg/m ³
0	590	Alluvium	590	Holocene	3,34	1483	2080
590	1800	Sand, Clay	1210	Pleistocene	2,45	1459	2100
1800	1985	Marly Limestone, Anhydrite	185	Messinian	3,05	785	2585
1985	5094	Marl, Conglomerate	3109	Tortonian	3,28	1359	2427
5094	5416	Limestone	322	Middle Eocene	2,6	921	2600
5416	5429	Marl	13	Albian	2,77	794	2278
5429	5445	Limestone	16	Barremian	2,6	921	2600
5445	6559	Dolomite,Limestone, Sandstone	1114	Rhaetian	3,15	953	2656

Table 3-4 Villafortuna 4

Top	Bottom	Lithology	Thickness (m)	Age	λ_s (W/mK)	$c_{p,s}$ (J/kg·K)	ρ (kg/m ³)
0	641	Alluvium	641	Holocene	3,34	1483	2080
641	1321	Sand, Clay, Sandstone, Marl	680	Pleistocene	2,67	1086	2340
1321	4560	Marl, Sandstone, Conglomerate	3239	Miocene	3,04	1182	2535
4560	5089	Marl, Sandstone	529	Eocene	3,1	1010	2505
5089	5967	Flysch, Marl, Dolomite, Limestone	878	Cretaceous	3,14	848	2473
5967	6323	Limestone	356	Ladinian	2,6	921	2600
6323	6453	Dolomite	130	Anisian	4,4	880	2763
6453	6551	Dolomite, Limestone, Sandstone	98	Anisian	3,5	901	2682

Table 3-5 Turbigio 1

Top	Bottom	Lithology	Thickness (m)	Age	λ_s W/mK	$c_{p,s}$ J/kg·K	ρ kg/m ³
0	610	Sand, Pebble & Clay	610	Quaternary	3,57	1764	1912
610	1201	Clay, Sand & Pebble	591	Pleistocene	3,57	1764	1912
1201	3017	Sand & Clay	1816	Miocene	2,45	1459	2100
3017	5400	Clay, Sandstone & Conglomerate	2383	Oligocene	3,28	1359	2427
5400	5421	Marl & Limestone	21	Eocene	2,7	794	2278
5421	5665	Marl, Sandstone & Limestone	244	Cretaceous	2,75	932	2416
5665	5917	Marl, Limestone, Dolomite, Flint	252	Jurassic	3,96	865	2547
5917	6633	Limestone, Dolomite, Marl, Sandstone	716	Triassic	3,21	1162	2324

The Villafortuna–Trecate case study was conducted by applying the CWHX configuration shown in Figure 3-2.

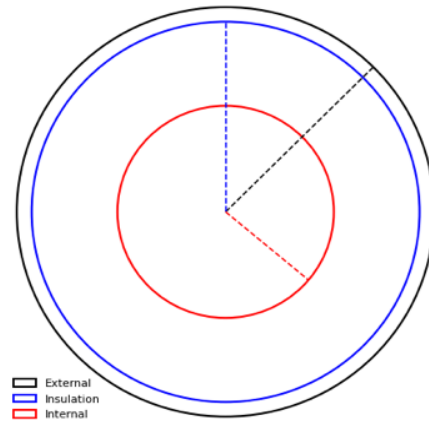


Figure 3-2 CWHX geometry: considered configuration [22].

To determine the most efficient design for the CWHX system, various configurations were implemented. These configurations are summarized in Table 3-6 [23–25]. The diameter size significantly influences fluid velocity. If the velocity is too low, the heat gained by the fluid in the downward pipe is lost in the upward pipe due to predominant convective exchange. Conversely, if the fluid moves too quickly, there isn't sufficient time for effective thermal exchange between the rocks and the fluid, resulting in a lower output temperature [23].

Table 3-6 Geometry of BHE

Study/Author	External Radius (mm)	Internal Radius (mm)	Insulation Radius (mm)
Alimonti (2016)	75.2	38.95	69.85
Blanke et al. (2021)	85	55	75
Bram et al. (1995)	122.25	53.67	117.78

3.4. Coaxial Wellbore Heat eXchanger Model

Using calculated thermal properties, a model was developed to estimate geothermal energy extraction and simulate CWHX system performance. This model integrates key parameters such as geothermal gradients, well depths, formation properties, fluid properties, and geometrical configuration [26–28]. Accurate modeling is essential for evaluating feasibility and optimizing the design of geothermal systems. The CWHX model operates on the assumption that heat transfer into the reservoir rock occurs through conduction, while heat transfer into the fluid within the tubes involves both conduction and convection. Recognizing the distinct behaviors in the descending and ascending flows within the coaxial tubes, a heat transfer model of the CWHX was developed using Python code.

3.4.1. Rock Temperature Evaluation

The temperature at depth Z was estimated based on the local geothermal gradient GT defined earlier, using the following equation:

$$T_s(Z) = T_g + GT \cdot Z \quad \text{Equation 1}$$

Here, T_g represents the mean ground surface temperature, which is assumed to be approximately 13°C in the case study area.

3.4.2. Transfer of Heat Within the Pipe System

3.4.2.1. Downward pipe

The fluid in the downward pipe (injection pipe) is in direct contact with the wall of the borehole. The pipe is made up of steel casing that is fixed into the rock wall with cement. The annular space between each pair of casings is filled with completion fluid or cement. It is believed that heat transfer from the reservoir rock to the borehole wall occurs via conduction, while heat transfer between the wall and the fluid occurs via convection. Convection into the reservoir rock is disregarded.

The fluid is in contact with the internal tube on the interior side of the downward pipe. Heat transfer between the two pipes primarily occurs through conduction within the pipe and via convection between the wall and the fluid.

The following equation represents the heat flux \dot{Q} transferred from the surrounding rock formation to the working fluid within the CWHX annulus [18].

$$\dot{Q}_{down} = 2\pi r_w \bar{U}_i (T_s(z) - T_{f,down}) \Delta L \quad \text{Equation 2}$$

where:

- r_w is the external radius of the borehole.
- \bar{U}_i is the total heat exchange coefficient.
- $T_s(z)$ is the rock temperature at depth z .
- $T_{f,down}$ is the temperature of the fluid in the injection pipe.
- ΔL is the variation in length of the pipe.

In the context of thermal resistance, the total heat exchange coefficient \bar{U}_i is the inverse of the total thermal resistance R_t expressed as $R_t = 1/\bar{U}_i$.

It represents the combined effect of various heat transfer mechanisms and can be formulated as the sum of thermal resistances, as shown in the equation:

$$R_t = R_a + R_c + R_s \quad \text{Equation 3}$$

where:

- R_a is the thermal resistance as a result of convective heat transmission into the pipe.
- R_c is the thermal resistance as a result of conductive heat transmission through the well completion casings.
- R_s is the thermal resistance as a result of conductive heat transmission in the rock, which changes over time.

The convective thermal resistance R_a is calculated as follows:

$$R_a = \frac{1}{2 \cdot r_c \cdot h_f} \quad \text{Equation 4}$$

where:

- r_c represents the radius of the external casing.
- h The convective heat transfer coefficient is determined using the definition of the Nusselt number, Nu .

$$h_f = \frac{Nu \cdot \lambda_f}{2 \cdot r_c} \quad \text{Equation 5}$$

and by applying the Dittuse-Boelter equation, under the assumption of turbulent flow inside the tubes (Reynolds number ≥ 104) [26]:

$$Nu = 0.023 \cdot \left(\frac{\rho \cdot v_f \cdot 2r_c}{\mu_f}\right)^{0.8} \cdot \left(\frac{c_{p,f} \cdot \mu_f}{\lambda_f}\right)^{0.4} \quad \text{Equation 6}$$

The following formula is used to calculate the rock's conductive thermal resistance R_s [29]:

$$R_s = \frac{1}{2\lambda_s} \ln \frac{r_s}{r_w} \quad \text{Equation 7}$$

where:

- λ_s is the rock's thermal conductivity.
- r_w is the well's external radius.
- r_s is the radius of thermal influence, defined as:

$$r_s = 2\sqrt{a_s t'} \quad \text{Equation 8}$$

where:

- t' is the time elapsed since the beginning
- a_s is the rock's thermal diffusivity, defined as:

$$\alpha_s = \frac{\lambda_s}{(\rho_s \cdot c_{p,s})} \quad \text{Equation 9}$$

where:

- ρ_s is the density of rock.
- $c_{p,s}$ is the specific heat capacity of rock.

As seen in Figure 3-3, the thermal influence radius of the CWHX grows extremely quickly over time. After 16 months of operation, the radius reaches 1 m and extends to just under 1.18 m after 9 years.

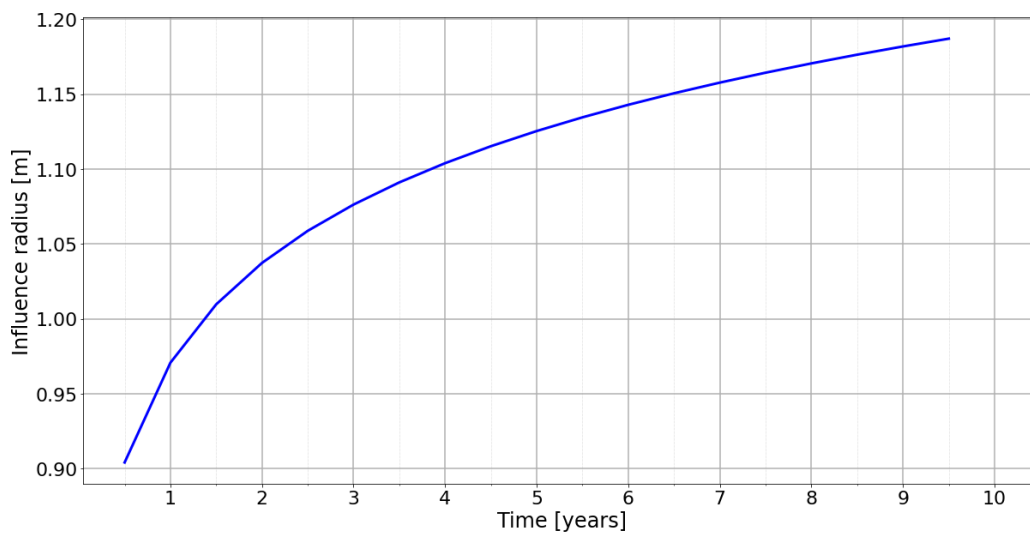


Figure 3-3 Thermal influence radius

The thermal resistance for heat conduction through the casings of the well completion R_c is calculated as follows:

$$R_c = \sum_{i=1}^n R_{\lambda i} = \frac{1}{2} \sum_{i=1}^n \frac{1}{\lambda_i} \ln \frac{r_{c,i+1}}{r_{c,i}} \quad \text{Equation 10}$$

The contribution of thermal resistance from the casings R_c is disregarded in the overall thermal resistance calculation, given the high thermal conductivity of the steel piping, which implies its negligible impact compared to the thermal resistance of the rock formation.

The model assumes $r_c = r_w$ for simplicity, since the pipes's thickness is negligible.

$$\frac{1}{U_i} = \frac{2 \cdot r_c}{2 \cdot \lambda_s} \cdot \ln \frac{r_s}{2 \cdot r_w} + \frac{1}{h} \quad \text{Equation 11}$$

3.4.2.2. Upward pipe

At the bottom of the well, the heated fluid flows into the internal pipe (extraction pipe). Heat exchange happens exclusively through the pipe wall as it approaches the wellhead.

The heat exchange is defined by the following equation:

$$\dot{Q}_{up} = 2\pi r_i U_e (T_{f,up} - T_{f,down}) \Delta L \quad \text{Equation 12}$$

where:

- r_i represents the radius of the extraction pipe.
- U_e is the extraction pipe's overall heat exchange coefficient.
- $T_{f,up}$ is the fluid temperature in the extraction pipe.
- $T_{f,down}$ is the fluid temperature in the injection pipe.
- ΔL is the variation in length of the pipe

In contrast to the downward (injection) pipe, the total heat exchange coefficient in the upward (extraction) pipe U_e , can be determined by applying the following relation, based on the theory of heat exchange in a multi-layer tubular wall:

$$\frac{1}{U_e} = \frac{r_i}{r_i + d} \cdot \frac{1}{h_o} + r_i \sum_{j=1}^n \ln\left(\frac{r_{j+1}}{r_j}\right) \cdot \frac{1}{\lambda_j} + \frac{1}{h_i} \quad \text{Equation 13}$$

The initial component in Equation 13 defines convective heat transfer to the exterior wall, where r_i represents the inner pipe radius, d is the composite pipe thickness, and h_o refers to the convective heat transfer coefficient to the exterior wall. Following this, the second segment corresponds to conductive heat exchange within the composite pipe, involving λ_j as the thermal conductivity and r_j as the material radius (air and steel). Lastly, the third term of the equation is attributed to convective heat transfer to the interior wall.

3.4.3. Heat Transfer Rate and Electrical Power Evaluation

Evaluating the heat transfer rate, also known as thermal power, and the subsequent electrical power generation in geothermal systems is critical for understanding system performance and efficiency. To assess the thermal power, the following equation is implemented:

$$Q = \dot{m} \cdot c_{p,w} \cdot \Delta T \quad \text{Equation 14}$$

where:

- \dot{m} represents the mass flow rate. This parameter significantly affects the heat transfer rate, as a higher mass flow rate can transport more thermal energy.
- $c_{p,w}$ is the specific heat capacity of water.
- ΔT is the temperature difference between the inlet and outlet of the system.

The electrical power W_e generated from the thermal energy can be evaluated using the efficiency η of the geothermal power conversion system:

$$W_e = Q \cdot \eta \quad \text{Equation 15}$$

where:

- W_e is the net electrical power output .
- η is the efficiency of the geothermal power conversion system, typically a percentage.
- Q is the thermal power input to the conversion system.

3.4.4. Pressure Losses and Pumping Power Consumption Evaluation

The WHX has been adjusted to generate maximum thermal power while minimizing the electrical power required for fluid pumping in the injection pipe. This optimization is facilitated by spontaneous circulation, driven by the thermosiphon effect. When the fluid is heated in the downward pipe, it naturally rises to the top through the extraction pipe. This is due to the pressure enhancement caused by the variation in density, which is lower in the downward pipe than in the upward pipe. Although pressure losses due to the extended length of the pipes is negligible, determining the total pressure loss is essential for calculating the required pumping energy and defining the system's efficiency. The pressure loss ΔP was assessed utilizing the Darcy-Weisbach equation with Petukhov's relation for the friction factor [30]:

$$\Delta P = \frac{L\rho_f v_f^2}{2D_h[0.79 \ln(Re) - 1.64]^2} \quad \text{Equation 16}$$

where:

- L is the length of the pipe.
- D_h the hydraulic diam, was determined as a function of the internal and external pipe diam [31].

The equation presumes turbulent flow in the entire pipe.

The electrical power required to circulate fluids W_{cp} needed for limiting the frictional pressure losses in the pipe determined as follows [32]:

$$W_{cp} = \frac{\Delta P \cdot \dot{m}}{\rho_f \cdot \eta} \quad \text{Equation 17}$$

where:

- \dot{m} represents the mass flow rate.
- η . represents the efficiency of the pump, which is assumed to be 70%.
- ρ_f represents the density of the fluid.

3.4.5. Assumptions and Estimations

In this study, Python, a powerful language enabling algorithmic solutions, has been implemented to conduct the simulation of the CWHX using the outlined model in various codes structured as shown in Figure 3-4.

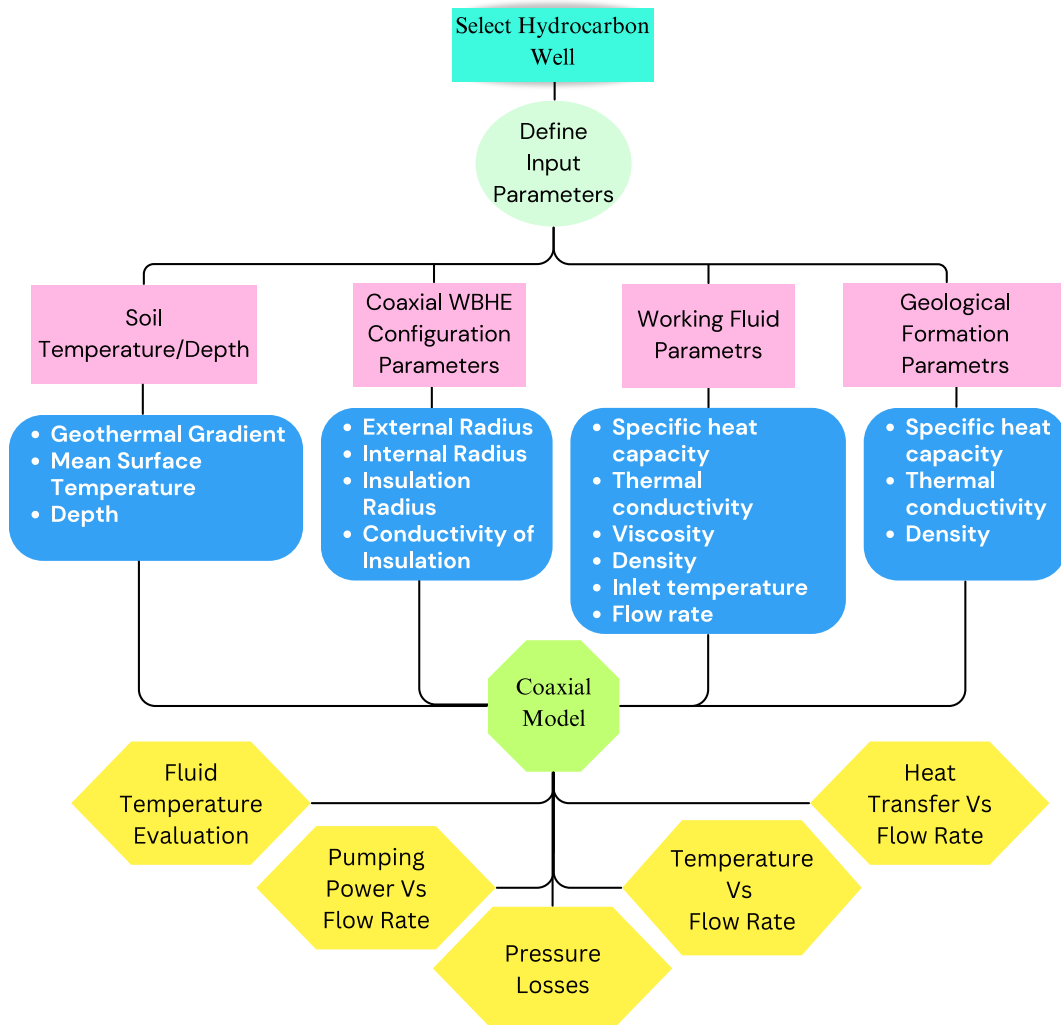


Figure 3-4 Flowchart modeling implemented using Python

The temperature profile is assumed to remain constant radially; therefore, there is no temperature variation within the annulus or the inner tube. However, temperature variations occur solely in the vertical direction within both the annulus and inner tube.

The attributes of the heat carrier fluid were considered constant, since water at 100°C and 2 bar selected for this research, no variations in pressure or temperature gradients were imposed. These specific values are reported in Table 3-7.

Table 3-7 Constant Fluid Properties

Fluid	Specific heat capacity (J/kg K)	Thermal conductivity (W/m K)	Viscosity (mmPa s)	Density (kg/m³)
Water	4186	0.679	0.28177	958.395

The analytical models assumed steady-state conditions, with no temperature variations over time and consistent temperatures at all points in the pipes. Additionally, the model assumed the resistance due to pipe thickness was insignificant, given the tube material's high conductivity, making its resistance minor compared to other system resistances.

The implied analytical model adopts a sequential approach, tracing the path of the working fluid. Specifically, it divides the system into intervals of length ΔL .

Chapter 4

4. Results and Discussion

In this chapter, we present the results of our analysis on the reuse of abandoned wells in the Villafortuna-Trecate oil field for geothermal purposes using a CWHX system. The study focuses on evaluating the thermal performance and efficiency of these wells under various configurations and flow rates. We aim to determine the optimal conditions for maximizing energy extraction while maintaining operational efficiency.

Here, we analyzed four different wells as our case studies, as shown in Table 3-1 in the Villafortuna-Trecate oil field. Specific heat capacity, thermal conductivity, and density were defined for each section of the formation related to each well, using the data in our model (Table 3-2, 3-3, 3-4, and 3-5). Three distinct configurations for our geothermal plant were evaluated, as outlined in Table 3-6. A consistent thermal conductivity value of 0.025 W/mK was maintained for the insulating material across all wells. Finally, water was selected as our carrier fluid with constant properties, as mentioned in Table 3-7, at three different flow rates: 1.5, 2.7, and 3 kg/s.

Using water has several benefits: it is not harmful to the subsurface in case of leakage, it has a good heat capacity rate, it is affordable and does not impose extra costs to the plant, it is accessible, and it requires less pumping energy for circulation compared to other carrier fluids.

The inlet water temperature was fixed for all wells, as they are located in the same region with an average temperature of approximately 15°C. It is assumed that the ground surface temperature and the water temperature at the surface are roughly equal. This value, supported by numerous references, was adopted as the fixed inlet temperature.

4.1. Long-Term CWHX System Performance

For evaluating the performance of the CWHX system over various time spans, we compared the outcomes of operating at a flow rate of 2.7 kg/s using the Alimonti configuration after both 2 and 10 years (Figure 4-1, Figure 4-2, Table 4-1, Table 4-2). This comparison yields insights into the system's long-term sustainability and efficiency.

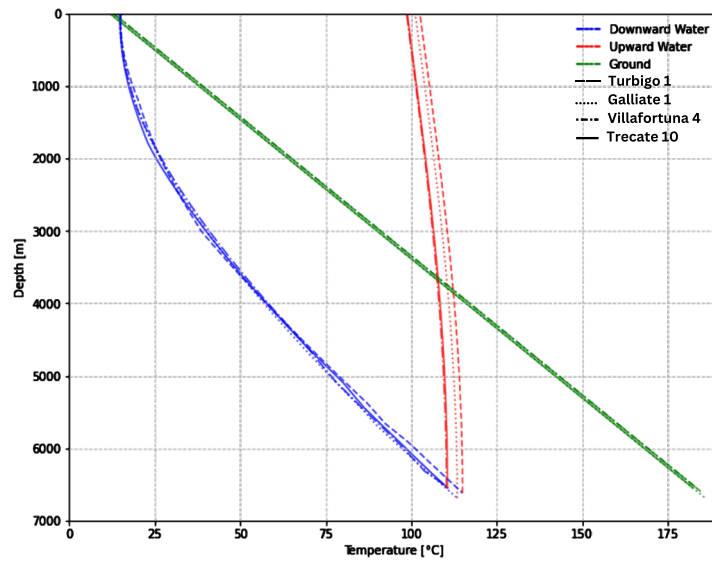


Figure 4-1 Performance Analysis *after 2 Years* for 2.7 kg/s Flow Rate with Alimonti Configuration

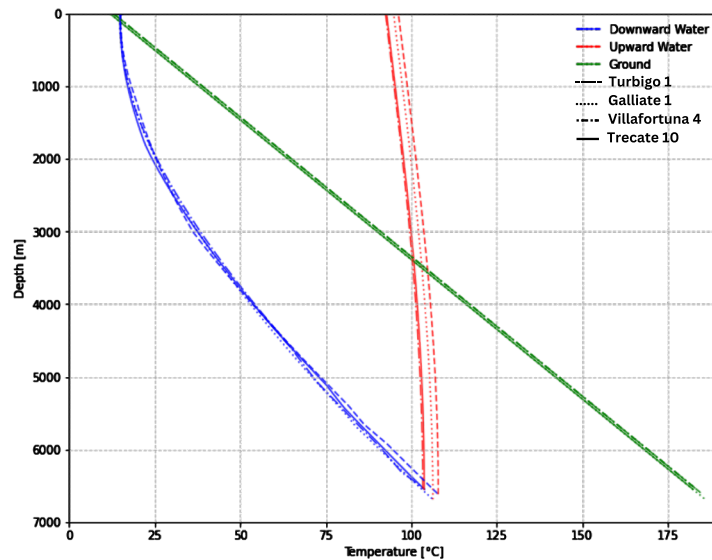


Figure 4-2 Performance Analysis *after 10 Years* for 2.7 kg/s Flow Rate with Alimonti Configuration

Table 4-1 Performance Metrics for 2.7 kg/s Flow Rate with Alimonti Configuration after 2 Years

Well	Bottomhole Temp (°C)	Surface Temp (°C)	ΔP (kPa)	Heat Transfer Rate (kW)	Wcp (kW)
Turbigo 1	115	103	720	989	2.8
Galliate 1	113	101	759	980	3.1
Trecate 10	111	99	712	947	2.8
Villafortuna 4	110	99	711	945	2.7

Table 4-2 Performance Metrics for 2.7 kg/s Flow Rate with Alimonti Configuration after 10 Years

Well	Bottomhole Temp (°C)	Surface Temp (°C)	ΔP (kPa)	Heat Transfer Rate (kW)	Wcp (kW)
Turbigo 1	107	96	730	977	2.8
Galliate 1	106	95	770	968	3.1
Trecate 10	104	93	723	932	2.8
Villafortuna 4	104	93	722	931	2.8

4.1.1. Comparison of 2-Year and 10-Year Performance

Temperature Trends: After 10 years, there is a noticeable decline in both bottomhole and surface temperatures across all wells. For example, Turbigo1’s bottomhole temperature decreased from 115°C to 108°C, and its surface temperature decreased from 103°C to 96°C. This trend indicates a gradual loss of thermal energy over time, which is expected as the geothermal system extracts heat from the ground.

Pressure Loss (ΔP): Pressure loss increased slightly after 10 years for all wells. For instance, Turbigo1’s pressure loss increased from 720 kPa to 730 kPa. This increase may be due to maintenance issues like corrosion and scaling, which can affect the resistance to fluid flow. Additionally, changes in the flow regime over time could contribute to the increased pressure loss. Long-term pipe friction is the primary cause of major losses in pipes, whereas component changes and other system changes are the cause of minor losses.

Heat Transfer Rate (Thermal Power): The heat transfer rate shows a minor reduction over 10 years. Turbigol's heat transfer rate decreased from 989 kW to 977 kW. This reduction reflects the decrease in temperature gradients as the system reaches a more thermally equilibrated state with the surrounding formation.

Power for Pumping (W_{cp}): The power required for pumping (W_{cp}) remained relatively stable, with only minor increases. For instance, Turbigol's W_{cp} increased from 2.78 kW to 2.81 kW. This indicates that while the efficiency of heat extraction decreases, the energy required to circulate the fluid remains largely unaffected.

In the long term, the efficiency of the geothermal system diminishes slightly, as evidenced by decreased temperatures and heat transfer rates over 10 years. Regular monitoring and potential adjustments in flow rates or operational strategies may be necessary to maintain optimal performance. However, the stable pumping power requirements support the sustainability of the system for long-term energy extraction. The Alimonti configuration with a flow rate of 2.7 kg/s demonstrates balanced performance with manageable declines in efficiency over a decade, making it suitable for long-term geothermal energy extraction with a good balance between heat extraction and operational costs. Further evaluation of other variables will be necessary, leading to comprehensive conclusions in the final thesis.

4.2. Flow Rate Impact on System Performance

To evaluate the impact of flow rates on the performance of the CWHX system, we analyzed the outcomes for different configurations across all wells after 2 years. Flow rates of 1.5 kg/s (5.4 m³/h), 2.7 kg/s (10 m³/h), and 5.56 kg/s (20 m³/h) were assessed to determine their effects on system efficiency. Figures are provided for the Alimonti configuration to visually illustrate key findings (Figure 4-3 to Figure 4-6), while numerical tables are used for the other configurations due to subtle differences not easily discernible in graphical form (Table 4-3, Table 4-4).

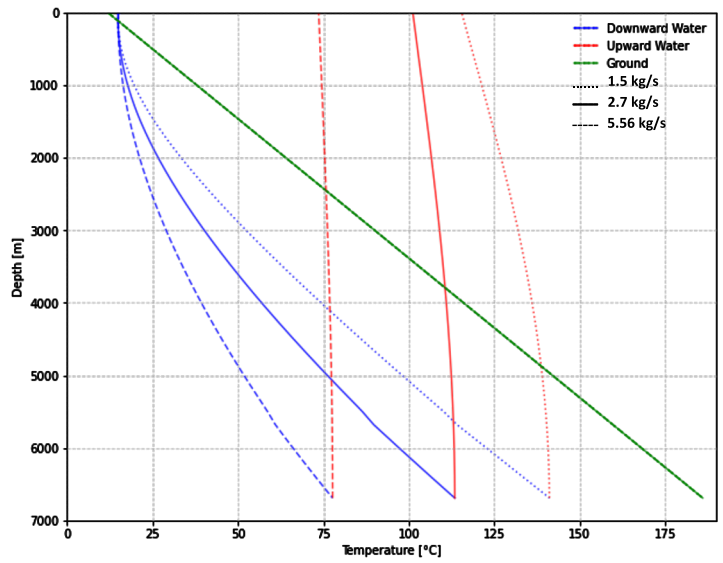


Figure 4-3 Performance analysis for **Galliate 1** with the Alimonti configuration at different flow rates

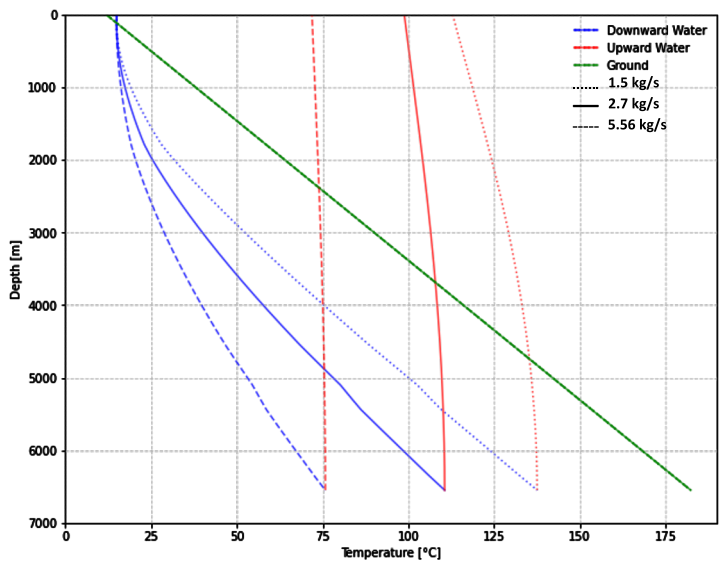


Figure 4-4 Performance analysis for **Trecate 10** with the Alimonti configuration at different flow rates

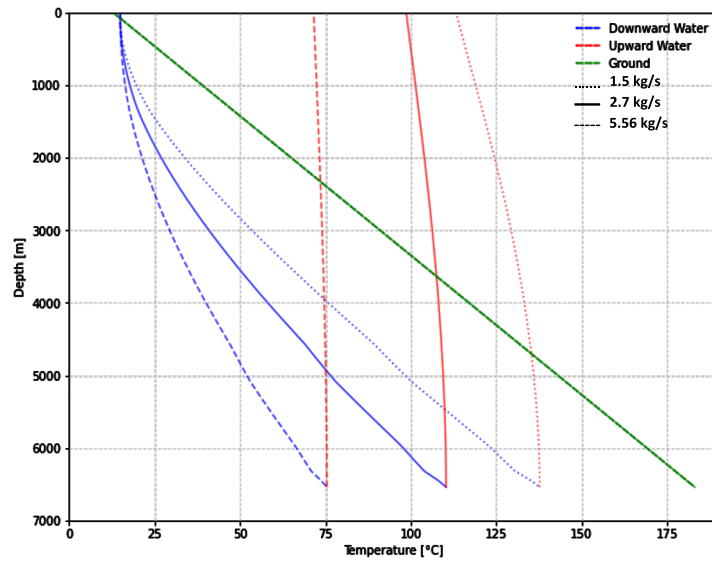


Figure 4-5 Performance analysis for *Villafortuna 4* with the Alimonti configuration at different flow rates

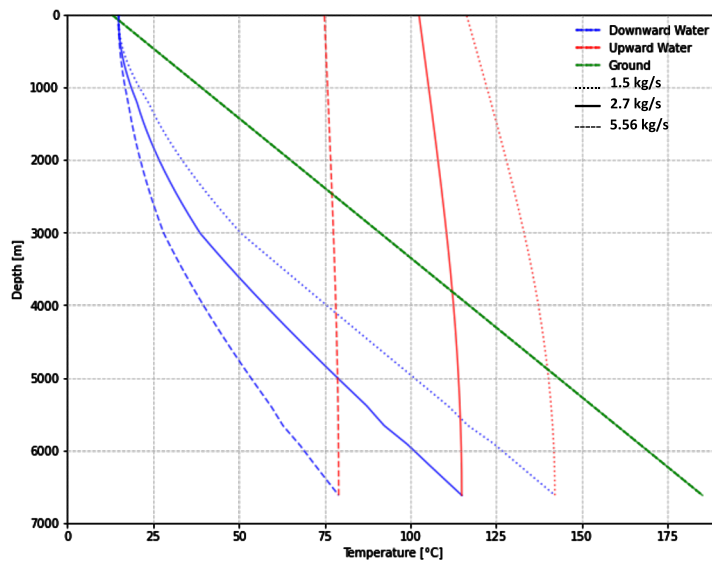


Figure 4-6 Performance analysis for *Turbigo 1* with the Alimonti configuration at different flow rates

4.2.1. Flow Rate Impact on Pressure Losses

A clear trend emerges when examining the relationship between flow rate and pressure drop. As the flow rate increases, the pressure drop (ΔP) across all wells and configurations rises significantly. For example, in Galliate 1, ΔP increases from approximately 200 kPa at 1.5 kg/s to over 3800 kPa at 5.56 kg/s across the Alimonti configuration (Table 4-3, Table 4-4). This behavior is expected, as higher flow rates

lead to increased frictional losses and higher velocities, both contributing to a greater pressure drop.

4.2.2. Flow Rate Impact on Temperature and Thermal Efficiency

The final temperatures at both the bottomhole and surface provide insights into thermal efficiency. As the flow rates increase, bottomhole temperatures decrease noticeably. For instance, at a lower flow rate of 1.5 kg/s, bottomhole temperatures range from 138°C to 146°C across various configurations. When the flow rate increases to 5.56 kg/s, these temperatures drop significantly to a range of 72°C to 84°C. Similarly, surface temperatures also decline with higher flow rates, as illustrated in Figure 4-7. For example, in Galliate 1 with the Alimonti configuration, surface temperatures drop from 115°C at 1.5 kg/s to 74°C at 5.56 kg/s.

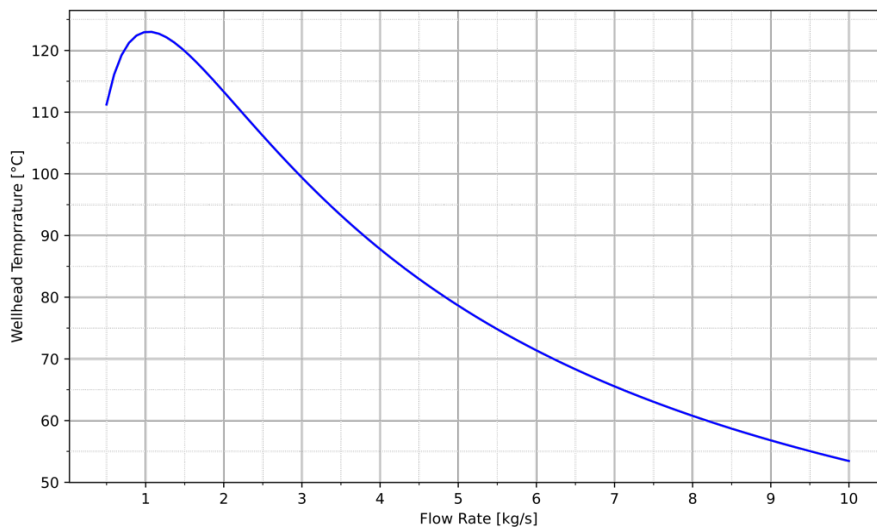


Figure 4-7 Impact of Flow Rate on Wellhead Temperature

This trend is consistent for all wells and configurations, indicates reduced thermal efficiency at higher flow rates. However, the heat transfer rate (thermal power) increases significantly with higher flow rates (Figure 4-8).

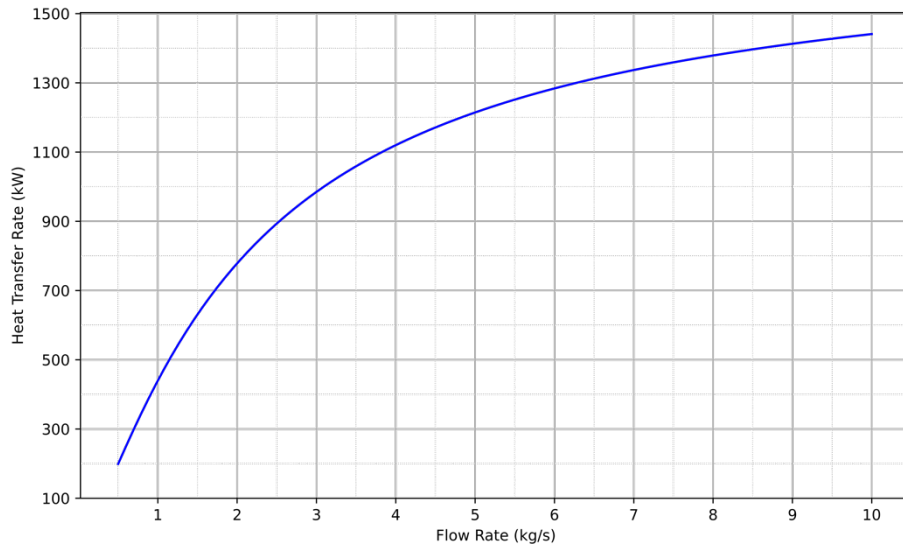


Figure 4-8 Impact of Flow Rate on Heat Transfer Rate (Thermal Power)

In the Galliate 1 well, for instance, the heat transfer rate rises from 635 kW at 1.5 kg/s to 1373 kW at 5.56 kg/s with the Alimonti configuration

This indicates that higher flow rates enhance the system’s ability to transfer heat despite the reduced temperatures. An optimal flow rate of 2.7 kg/s strikes a balance between effective heat extraction and maintaining manageable temperature profiles.

4.2.3. Flow Rate Impact on Pumping Power (W_{cp})

The pumping power required to circulate the fluid within the system (W_{cp}) significantly increases with higher flow rates (Figure 4-9). At 1.5 kg/s, W_{cp} values are low, e.g., 0.45 kW in the Galliate 1 well (Alimonti configuration). At the highest flow rate of 5.56 kg/s, W_{cp} values jump dramatically, reaching up to 32.0 kW in the same well and configuration (Table 4-3, Table 4-4). This indicates that while higher flow rates improve heat transfer, they also demand substantially more power for fluid circulation, impacting the overall system efficiency and operational costs.

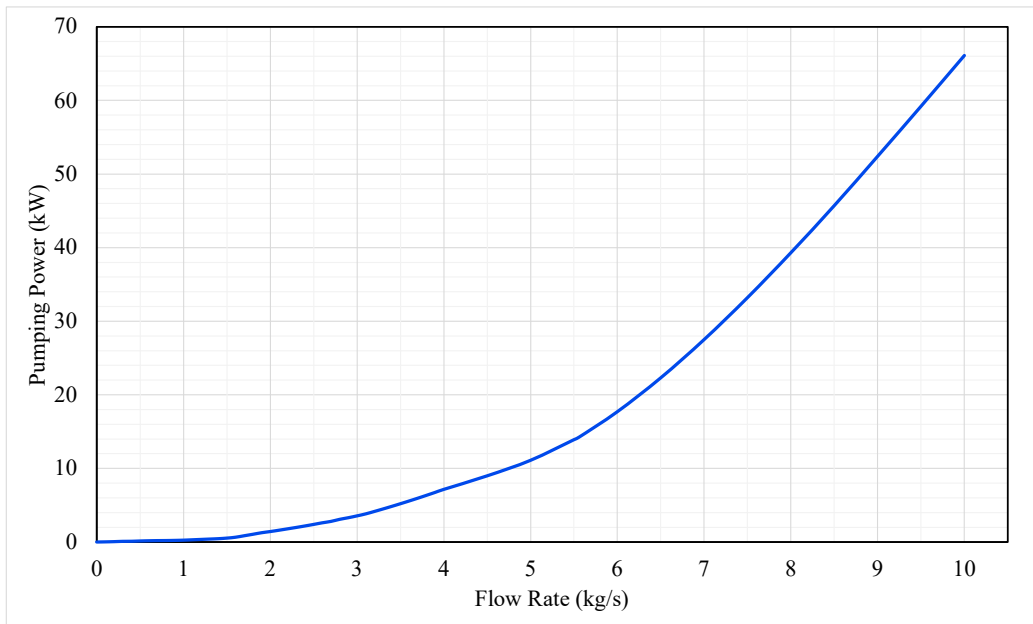


Figure 4-9 Impact of Flow Rate on Pumping Power Required (W_{cp})

4.3. Configuration Impact on System Performance

Selecting the optimal configuration depends on specific project requirements, balancing thermal efficiency, operational costs, and heat transfer performance across different flow rates and wells. Various configurations were evaluated in order to determine which CWHX model is more efficient (Table 4-3, Table 4-4). In this section, we analyze the different impacts of changing the system's configuration.

Pressure Loss (ΔP): Bram generally exhibits lower pressure losses compared to Alimonti and Blanke configurations across all flow rates and wells. This suggests Bram could be more efficient in terms of fluid circulation resistance. However, as evident from Table 4-3, Table 4-4, the influence of geometry on pressure loss is minimal. The dominant factor affecting pressure loss is the flow rate, which correlates directly with frictional losses.

Temperature Profiles: Alimonti tends to show higher bottomhole temperatures but lower surface temperatures compared to Blanke and Bram configurations. This indicates differences in heat extraction efficiencies and surface heat dissipation (Figure 4-10 to Figure 4-13).

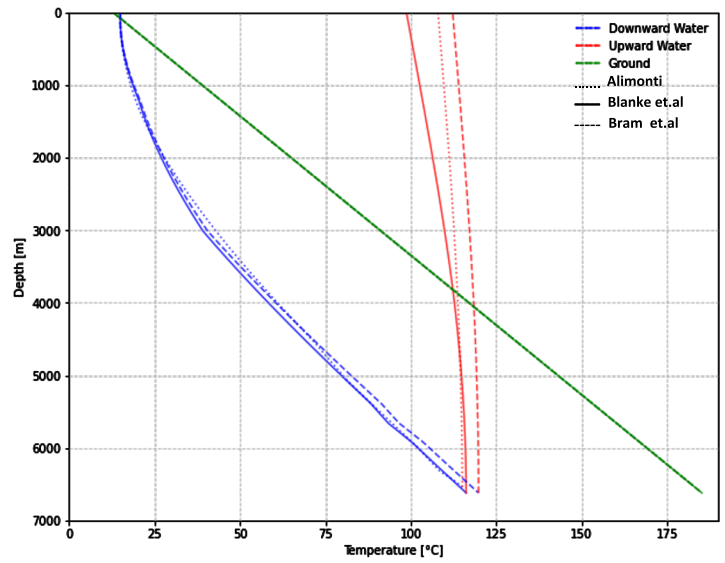


Figure 4-10 Performance Analysis for **Turbigo1** at 2.7 kg/s Flow Rate & Different Configurations

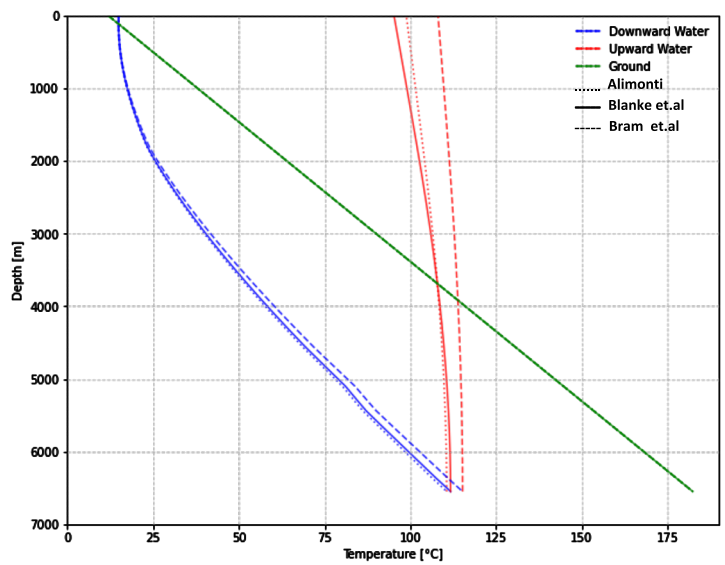


Figure 4-11 Performance Analysis for **Trecate10** at 2.7 kg/s Flow Rate & Different Configurations

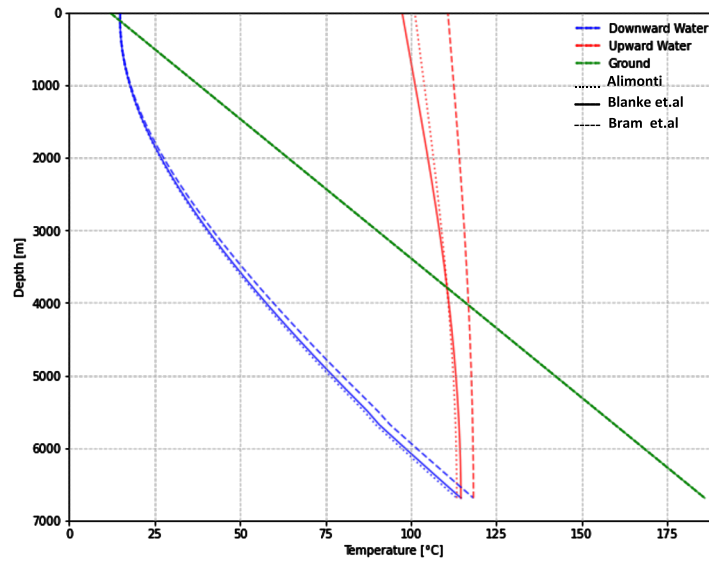


Figure 4-12 Performance Analysis for *Galliate1* at 2.7 kg/s Flow Rate & Different Configurations

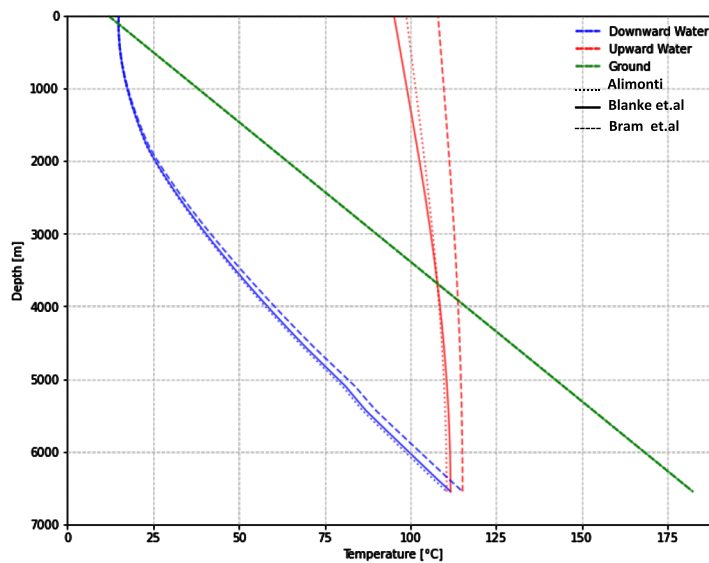


Figure 4-13 Performance Analysis for *Villafortuna4* at 2.7 kg/s Flow Rate & Different Configurations

Heat Transfer Rate: Across different flow rates and wells, Bram consistently demonstrates higher heat transfer rates compared to Alimonti and Blanke configurations. This suggests that Bram configuration may have better heat transfer capabilities due to its geometry and design parameters.

Pumping Power (W_{cp}): Alimonti generally requires lower pumping power (W_{cp}) compared to Blanke and Bram configurations, especially noticeable at higher flow rates. This indicates that Alimonti could be more energy-efficient in terms of fluid circulation, despite potentially lower heat transfer rates.

Overall Efficiency: The optimum configuration is defined as the one that maximizes thermal efficiency while minimizing circulation energy demand and operational costs. Alimonti offers a balance with lower W_{cp} and higher bottomhole temperatures, suitable for applications prioritizing thermal efficiency. Bram excels in heat transfer rate but may require higher W_{cp} , making it suitable for scenarios where maximizing heat extraction is crucial despite increased operational costs. Blanke configuration falls between the two, offering moderate performance in both heat transfer and W_{cp} .

It is noted that since the wellbores already exist, we cannot change the outer diameter of the wells. The Alimonti configuration is suggested based on the average diameter of wells located in the Villafortuna-Trecate oil field [23].

Table 4-3 Simulation Results for Different Wells, Flow Rates, and Geometry Configurations

Well Name	Flow Rate (kg/s)	Geometry Config.	ΔP (kPa)	Bottomhole Temp (°C)	Surface Temp (°C)	Heat Transfer Rate (kW)	Wcp (kW)
Galliate 1	1.5	Alimonti	201	141	115	635	0.44
		Blanke	201	142	107	583	0.48
		Bram	177	145	129	723	0.39
	2.7	Alimonti	759	113	101	980	3.05
		Blanke	761	115	97	938	3.1
		Bram	675	118	111	1090	2.72
	5.56	Alimonti	3829	78	74	1373	31.7
		Blanke	3856	79	73	1357	32.0
		Bram	3454	82	80	1514	28.6
Trecate 10	1.5	Alimonti	189	138	113	615	0.4
		Blanke	189	138	105	564	0.4
		Bram	166	141	126	698	0.36
	2.7	Alimonti	712	111	99	947	2.75
		Blanke	715	112	95	907	2.76
		Bram	634	115	108	1052	2.45
	5.56	Alimonti	3595	76	72	1324	28.6
		Blanke	3621	77	71	1308	28.8
		Bram	3243	80	78	1457	25.8

Table 4-4 Simulation Results for Different Wells, Flow Rates, and Geometry Configurations

Well Name	Flow Rate (kg/s)	Geometry Config.	ΔP (kPa)	Bottomhole Temp (°C)	Surface Temp (°C)	Heat Transfer Rate (kW)	Wcp (kW)
Turbigo 1	1.5	Alimonti	190	142	116	636	0.40
		Blanke	190	143	108	584	0.41
		Bram	168	146	130	723	0.36
	2.7	Alimonti	720	115	103	989	2.78
		Blanke	722	116	99	946	2.79
		Bram	641	120	112	1099	2.47
	5.56	Alimonti	3632	79	75	1395	28.9
		Blanke	3657	80	74	1378	29.0
		Bram	3276	84	81	1536	26.0
Villafortuna 4	1.5	Alimonti	188	138	113	616	0.4
		Blanke	188	139	105	567	0.41
		Bram	166	142	127	700	0.35
	2.7	Alimonti	711	110	99	945	2.74
		Blanke	714	111	95	906	2.75
		Bram	633	115	108	1050	2.44
	5.56	Alimonti	3591	75	72	1316	28.5
		Blanke	3615	76	71	1301	28.7
		Bram	3238	80	77	1449	25.7

4.4. The Impact of Flow Rate and Configuration on Thermal and Electrical Power Generation

4.4.1. Thermal Power Generation

This section examines how variations in flow rate and well configuration influence thermal power generation. Table 4-5 illustrates the summation of thermal power outputs at various flow rates and configurations of wells (Galliate 1, Trecate 10, Turbigio 1, and Villafortuna 4).

Table 4-5 Summation of Thermal Power Outputs for Different Flow Rates & Configurations of all 4 wells

Flow Rate (kg/s)	Alimonti (kW)	Blanke (kW)	Bram (kW)
1.5	2503	2297	2844
2.7	3862	3697	4291
5.56	5408	5344	5955

Data analysis reveals that the Bram configuration consistently yields the highest thermal power generation, followed by Alimonti and then Blanke, across various flow rates. This suggests Bram's superior efficiency in converting geothermal energy. However, considering practical constraints and the existing well infrastructure, the Alimonti configuration is the most suitable option to maximize thermal power output.

4.4.2. Electrical Power Generation

To estimate the total daily electrical power generated W_e for different flow rates and configurations by the CWHX across all four wells, we implemented Equation 15, assuming a system efficiency of 15%. The results are illustrated in Table 4-6.

Table 4-6 Total Daily Electrical Power Generated for Different Flow Rates & Configurations of all wells

Flow Rate (kg/s)	Alimonti (MWh)	Blanke (MWh)	Bram (MWh)
1.5	9.008	8.266	10.235
2.7	13.897	13.329	15.484
5.56	19.468	19.270	21.422

Considering the negligible contribution of pumping power to the net electrical output, the resulting daily electrical energy generated (MWh) from the geothermal wells is presented. This energy can be utilized for various applications.

4.5. Possible Application of Case Studies

The daily electrical power values generated from the wells demonstrate substantial potential across various applications. The following section outlines some potential uses based on the generated power.

4.5.1. Potential Applications for Generated Electrical Power

Residential Power Supply: The electrical output ranging from 9.008 to 21.422 MW can supply a substantial number of households. With an average household consumption of approximately 0.9 kW per hour, these power values are capable of supporting thousands of homes. Specifically, 9.008 MW can supply around 10,000 homes, and 21.422 MW can provide for approximately 24,000 homes. Considering Romentino, Trecate, Cameri, and Galiat have a total population of approximately 50,000 people, assuming an average of 3 residents per household, these four wells alone could potentially supply the electrical needs of about 17,000 homes located near the field.

Industrial Use: These power values are suitable for powering small to medium-sized manufacturing plants, which typically require 2-5 MW and 5-20 MW, respectively, or processing facilities.

Electric Vehicle Charging Stations: Electric Vehicle Charging Stations: Large-scale EV charging stations, crucial for public transport fleets or corporate vehicle fleets, can be sustained by these power levels. A large EV charging station typically requires between 1 and 10 MW.

4.5.1.1. Example Applications Based on Specific Values

- **9.008 MW (Lowest Value - Alimonti, 1.5 kg/s):**
 - a) Can power a small residential community of around 10,000 homes.
 - b) Enabled to run a medium-sized production plant.

- **13.897 MW (Medium Value - Alimonti, 2.7 kg/s):**
 - a) It is capable of supplying power to a large office building complex or a small data center.
 - b) Suitable for a small to medium-sized desalination plant.
- **21.422 MW (Highest Value - Bram, 5.56 kg/s):**
 - a) Can support a larger residential area of around 24,000 homes.
 - b) It has the capacity to power a medium to large data center or a large industrial facility.
 - c) Suitable for a significant portion of a public transport system or a large EV charging station.

4.5.2. Potential Applications for Generated Thermal Power

While the electrical power generated from the wells may be overestimated and not comparable to conventional geothermal power plants, this is a recognized limitation of the CWHX technology. However, based on numerical estimates of thermal power generation and output temperatures, the potential use for district heating plants is promising and can be assured. Typically at temperatures between 70°C and 90°C, can supply residential and commercial buildings, reducing reliance on fossil fuels and lowering emissions, similar to the systems used in Reykjavik, Iceland.

Additionally, in greenhouse agriculture, geothermal heat typically around 60°C to 80°C supports year-round cultivation, reduces energy costs, and extends growing seasons, as practiced in the Netherlands. In industrial processes, geothermal heat at temperatures of 60°C to 100°C is used in food processing, textile manufacturing, and paper mills for drying, pasteurization, and other processes, exemplified by Italy's dairy industry.

4.6. Limitations and Challenges

While the results of this study demonstrate the potential of using abandoned geothermal wells for thermal power generation, several limitations and challenges need to be acknowledged:

- **Pre-existing Well Characteristics:** Since these abandoned wells already exist, it would be difficult or costly to alter their diameters or make them deeper. The fixed dimensions of the wellbore may restrict the efficiency and capacity of the thermal energy extraction process.

- **Corrosion and Material Degradation:** Over time, corrosion may occur due to prolonged exposure to hot water. This can damage the wellbore and associated infrastructure, leading to increased maintenance costs and potential downtime.

- **Thermal Behaviour of the Formation:** Examining the thermal behaviour of the geological formation far from the wellbore is critical to ensure the sustainability of the system. Without a comprehensive understanding of the thermal conductivity and heat capacity of the surrounding rock, there is a risk of thermal depletion, which could reduce the efficiency of the heat extraction process over time.

- **Access to Data Limitations:** Access to data on abandoned wells is limited due to regulatory restrictions and national security concerns, particularly in oil and gas-dominated regions. Companies may withhold information due to compliance or national security mandates. This lack of transparency makes it difficult to assess the potential of these wells for repurposing, such as for geothermal energy production. Addressing these limitations requires international collaboration, regulatory reforms, and transparent data-sharing frameworks.

- **Energy Storage:** Storing the thermal energy generated from geothermal wells for use during peak demand times presents another challenge. Developing efficient thermal energy storage systems, such as insulated tanks or underground reservoirs, is essential to balance supply and demand.

- **Integration with Existing Infrastructure:** Integrating geothermal energy systems with existing infrastructure, such as district heating networks or industrial processes, can be complex. It requires careful planning and coordination to ensure compatibility and efficiency.

- **Geological Uncertainty:** There is always an element of uncertainty with geological formations. Unexpected geological conditions can affect the performance and lifespan of geothermal wells. Continuous geological assessments and adaptive management strategies are necessary to address this uncertainty.

Chapter 5

5. Conclusion

The study conducted on the reuse of abandoned wells in the Villafortuna-Trecate oil field as geothermal resources demonstrates significant potential, alongside several challenges that need to be addressed for successful implementation. This chapter summarizes the key findings and conclusions.

5.1. Key Findings

- **Thermal Performance and Efficiency:**

The analysis indicated that among the configurations tested, the Bram configuration consistently achieved higher heat transfer rates (thermal power) compared to Alimonti and Blanke configurations. However, it also required higher pumping power (W_{cp}), which may lead to increased operational costs.

The Alimonti configuration, while having lower heat transfer rates, showed greater energy efficiency due to its lower pumping power requirements. This configuration is recommended for scenarios where operational cost minimization is crucial.

- **Optimal Flow Rate:**

The optimal flow rate identified was 2.7 kg/s, balancing effective heat extraction and maintaining manageable temperature profiles. Higher flow rates, although increasing heat transfer rates, resulted in reduced thermal efficiency and significantly higher pumping power requirements. Computational results indicate that the geothermal energy produced from abandoned wells depends largely on the flow rate of fluid and the geothermal gradient, and the geometry of the wellbore.

- **Sustainability and Long-Term Performance:**

Long-term performance analysis at a flow rate of 2.7 kg/s using the Alimonti configuration over 2 and 10 years revealed the system's potential sustainability. The system demonstrated stable thermal performance, indicating its viability for long-term geothermal energy extraction.

- **Potential Applications:**

The thermal power generated is suitable for district heating applications, with temperatures between 70°C and 90°C effective for residential and commercial heating. Geothermal heat at 60°C to 80°C supports greenhouse agriculture, and 60°C to 100°C can be used in various industrial processes.

- **Coaxial Wellbore Heat eXchanger (CWHX):**

The Coaxial Wellbore Heat Exchanger (CWHX) enables heat extraction without producing geothermal fluids, reducing environmental impact and reinjection energy, and avoiding corrosion and scale issues. However, it has reduced heat recovery efficiency. This study evaluated and confirmed the feasibility of implementing the CWHX in the Villafortuna-Trecate oilfield, with the extracted heat potentially used for district heating and electrical energy production.

5.2. Future Work

To build upon the findings of this research and address the identified challenges, several areas of future work are recommended:

- **Advanced Material Research:**

Investigate and develop advanced materials with higher resistance to corrosion and thermal degradation. This will enhance the longevity and reliability of geothermal systems, particularly in harsh environments.

- **Enhanced Thermal Simulation Models:**

Develop more sophisticated thermal simulation models that incorporate real-time data and predictive analytics. Enhancing the precision of the suggested models by means of future assessment is necessary. The basic assumption related to the constancy of the properties of the water as working fluid must be overcome by

properly analyzing the possibility of having phase change (evaporation) in the well, which would change the suggested models. It is also necessary to carefully analyze the function of heat extraction from abandoned wells of intraformational flows and its impact on heat transfer.

- **Pilot Projects and Field Tests:**

Implement pilot projects in different geological settings to validate theoretical models and laboratory findings. Field tests will provide valuable data on real-world performance, operational challenges, and economic feasibility.

- **Economic Analysis and Cost-Benefit Studies:**

Conduct comprehensive economic analyses to compare the costs and benefits of geothermal energy against other renewable energy sources. These studies should consider long-term operational costs, environmental benefits, and potential for job creation. After a preliminary analysis about the presence of industries and agricultural districts, it will be useful to produce a detailed evaluation of the industrial plants available in the area near the wellbores: a technical feasibility and cost-benefit analysis of the selected configuration in this proposed case study could represent the subject of future research work.

- **Non-Aqueous Working Fluids:**

The efficiency of the system can be improved by using a non-aqueous working fluid such as Isobutane, Freon, and Ammonia as they vaporize to steam at a lower temperature due to their lower boiling point.

By focusing on these areas, future research and development can enhance the viability and efficiency of using abandoned wells as geothermal resources. This will contribute to a more sustainable and resilient energy system, supporting global efforts to transition to renewable energy sources and reduce carbon emissions.

References:

- [1] IEA. "Renewables 2019." IEA, Paris, 2019.
<https://www.iea.org/reports/renewables-2019>. Licence: CC BY 4.0.
- [2] Intergovernmental Panel on Climate Change (IPCC). Accessed June 11, 2024. <https://www.ipcc.ch/sr15>.
- [3] Jolie E, Scott S, Faulds J, Chambefort I, Axelsson G, Gutiérrez-Negrín LC, et al. Geological controls on geothermal resources for power generation. *Nat Rev Earth Environ* 2021;2:324–39. <https://doi.org/10.1038/s43017-021-00154-y>.
- [4] Lund JW, Freeston DH, Boyd TL. Direct utilization of geothermal energy 2010 worldwide review. *Geothermics* 2011;40:159–80. <https://doi.org/10.1016/J.GEOTHERMICS.2011.07.004>.
- [5] Ito T, Ruiz C, International Renewable Energy Agency. Geothermal power : technology brief n.d.:23.
- [6] Kaczmarczyk M, Tomaszewska B, Operacz A. Sustainable Utilization of Low Enthalpy Geothermal Resources to Electricity Generation through a Cascade System. *Energies (Basel)* 2020;13:2495. <https://doi.org/10.3390/en13102495>.
- [7] Manzella A, Serra D, Cesari G, Bargiacchi E, Cei M, Cerutti P, et al. Geothermal Energy Use, Country Update for Italy. *European Geothermal Congress 2019 Den Haag*; 2019.
- [8] Enel Green Power. "Geothermal Energy in Italy." Accessed June 11, 2024. <https://www.enelgreenpower.com/learning-hub/renewable-energies/geothermal-energy/italy>.
- [9] Bertello F, Fantoni R, Franciosi R, Gatti V, Ghielmi M, Pugliese A. From thrust-and-fold belt to foreland: hydrocarbon occurrences in Italy. *Geological Society, London, Petroleum Geology Conference Series* 2010;7:113–26. <https://doi.org/10.1144/0070113>.

- [10] Enzo Zappaterra (2). Source-Rock Distribution Model of the Periadriatic Region. *Am Assoc Pet Geol Bull* 1994;78. <https://doi.org/10.1306/BDF90A0-1718-11D7-8645000102C1865D>.
- [11] Moustafa AM, Shehata AS, Shehata AI, Hanafy AA. Reuse of Abandoned oil and gas wells for Power generation in Western Dessert and Gulf of Suez fields of Egypt. *Energy Reports* 2022;8:1349–60. <https://doi.org/10.1016/j.egy.2022.07.067>.
- [12] Casero, P. "Special Volume of the Italian Geological Society for the IGC 32 Florence.
- [13] Pasquale V, Chiozzi P, Verdoya M, Gola G. Heat flow in the Western Po Basin and the surrounding orogenic belts. *Geophys J Int* 2012;190:8–22. <https://doi.org/10.1111/j.1365-246X.2012.05486.x>.
- [14] Alimonti C, Gnoni AA. Harnessing the fluids heat to improve mature oil field: The Villafortuna-Trecate case study. *J Pet Sci Eng* 2015;125:256–62. <https://doi.org/10.1016/j.petrol.2014.11.029>.
- [15] Turrini C, Bosica B, Ryan P, Shiner P, Lacombe O, Roure F. 3D structural and thermal modelling of Mesozoic petroleum systems in the Po Valley Basin, northern Italy 3D structural and thermal modelling of Mesozoic petroleum systems in the Po. Valley Basin, Northern Italy *Petroleum Geoscience* 2018;24:172. <https://doi.org/10.1144/petgeo2017-031i>.
- [16] Alimonti C, Gnoni AA. Harnessing the fluids heat to improve mature oil field: The Villafortuna–Trecate case study. *J Pet Sci Eng* 2015;125:256–62. <https://doi.org/10.1016/j.petrol.2014.11.029>.
- [17] Angliviè de La Beaumelle N, Blok K, de Chalendar JA, Clarke L, Hahmann AN, Huster J, et al. The Global Technical, Economic, and Feasible Potential of Renewable Electricity. *Annu Rev Environ Resour* 2023;48:419–49. <https://doi.org/10.1146/annurev-environ-112321-091140>.
- [18] Gizzi M, Taddia G, Russo S Lo. Reuse of Decommissioned Hydrocarbon Wells in Italian Oilfields by Means of a Closed-Loop Geothermal System 2021. <https://doi.org/10.3390/app11052411>.

- [19] Geothermal energy in the CNR. <https://geothopica.igg.cnr.it/index.php/it/chi-siamo/geotermia-nel-cnr> (accessed June 11, 2024).
- [20] Hamdhan, I.N., and B.G. Clarke. "Determination of Thermal Conductivity of Coarse and Fine Sand Soils." 2010.
- [21] Pasquale V, Gola G, Chiozzi P, Verdoya M. Thermophysical properties of the Po Basin rocks. *Geophys J Int* 2011;186:69–81. <https://doi.org/10.1111/j.1365-246X.2011.05040.x>.
- [22] Gizzi M, Taddia G, Lo Russo S. Reuse of Decommissioned Hydrocarbon Wells in Italian Oilfields by Means of a Closed-Loop Geothermal System. *Applied Sciences* 2021;11:2411. <https://doi.org/10.3390/app11052411>.
- [23] Alimonti C, Soldo E. Study of geothermal power generation from a very deep oil well with a wellbore heat exchanger. *Renew Energy* 2016;86:292–301. <https://doi.org/10.1016/j.renene.2015.08.031>.
- [24] Blanke T, Hagenkamp M, Döring B, Göttsche J, Reger V, Kuhnhenne M. Net-exergetic, hydraulic and thermal optimization of coaxial heat exchangers using fixed flow conditions instead of fixed flow rates. *Geothermal Energy* 2021;9. <https://doi.org/10.1186/s40517-021-00201-3>.
- [25] "Bram K, "Draxler J, "Hirschmann G, "Zoth Geological Survey Hannover (Germany)]" G [KTB CDDPMG, "Hiron Schlumberger Riboud Product Clamart (France)]" S [Pressure SS, "Kuehr Windischeschenbach (Germany)]" M [Schlumberger W and TN. The KTB Borehole-Germany's superdeep telescope into the earth crust 1995;7. <https://doi.org/https://doi.org/>.
- [26] Davis AP, Michaelides EE. Geothermal power production from abandoned oil wells. *Energy* 2009;34:866–72. <https://doi.org/10.1016/j.energy.2009.03.017>.
- [27] Cheng W-L, Li T-T, Nian Y-L, Wang C-L. Studies on geothermal power generation using abandoned oil wells. *Energy* 2013;59:248–54. <https://doi.org/10.1016/j.energy.2013.07.008>.

- [28] Bu X, Ma W, Li H. Geothermal energy production utilizing abandoned oil and gas wells. *Renew Energy* 2012;41:80–5. <https://doi.org/10.1016/j.renene.2011.10.009>.
- [29] Kujawa, T.; Nowak, W.; Stachel, A.A. Utilization of existing deep geological wells for acquisitions of geothermal energy. *Energy* 2006, 31, 650–664.
- [30] Brown CS, Kolo I, Banks D, Falcone G. Comparison of the thermal and hydraulic performance of single U-tube, double U-tube and coaxial medium-to-deep borehole heat exchangers. *Geothermics* 2024;117:102888. <https://doi.org/10.1016/J.GEOTHERMICS.2023.102888>.
- [31] Fluid Flow - Hydraulic Diameter." Accessed June 11, 2024. https://www.engineeringtoolbox.com/hydraulic-equivalent-diameter-d_458.html).
- [32] Liu J, Wang F, Cai W, Wang Z, Wei Q, Deng J. Numerical study on the effects of design parameters on the heat transfer performance of coaxial deep borehole heat exchanger 2019. <https://doi.org/10.1002/er.4357>.